The curious case of Mercury's internal structure

JOURNAL OF GEOPHYSICAL RESEARCH: PLANETS, VOL. 118, 1204–1220, doi:10.1002/jgre.20091, 2013

The curious case of Mercury's internal structure

Steven A. Hauck II,[1] Jean-Luc Margot,[2,3] Sean C. Solomon,[4,5] Roger J. Phillips,[6] Catherine L. Johnson,[7,8] Frank G. Lemoine,[9] Erwan Mazarico,[10] Timothy J. McCoy,[11] Sebastiano Padovan,[3] Stanton J. Peale,[12] Mark E. Perry,[13] David E. Smith,[10] and Maria T. Zuber[10]

Received 29 June 2012; revised 21 February 2013; accepted 3 May 2013; published 5 June 2013.

[1] The recent determination of the gravity field of Mercury and new Earth-based radar observations of the planet's spin state afford the opportunity to explore Mercury's internal structure. These observations provide estimates of two measures of the radial mass distribution of Mercury: the normalized polar moment of inertia and the fractional polar moment of inertia of the solid portion of the planet overlying the liquid core. Employing Monte Carlo techniques, we calculate several million models of the radial density structure of Mercury consistent with its radius and bulk density and constrained by these moment of inertia parameters. We estimate that the top of the liquid core is at a radius of 2020 ± 30 km, the mean density above this boundary is $3380 \pm 200\,\mathrm{kg\,m^{-3}}$, and the density below the boundary is $6980 \pm 280\,\mathrm{kg\,m^{-3}}$. We find that these internal structure parameters are robust across a broad range of compositional models for the core and planet as a whole. Geochemical observations of Mercury's surface by MESSENGER indicate a chemically reducing environment that would favor the partitioning of silicon or both silicon and sulfur into the metallic core during core-mantle differentiation. For a core composed of Fe–S–Si materials, the thermodynamic properties at elevated pressures and temperatures suggest that an FeS-rich layer could form at the top of the core and that a portion of it may be presently solid.

Citation: Hauck, S. A., II. et al. (2013), The curious case of Mercury's internal structure, *J. Geophys. Res. Planets*, *118*, 1204–1220, doi:10.1002/jgre.20091.

1. Introduction

[2] The organization of a planet's interior is a crucial indicator of its formation and early history and provides fundamental constraints on how the planet has evolved. The high bulk density of the planet Mercury has long suggested that the planet's average composition is more enriched in metallic iron than the other terrestrial planets. Prior to the insertion of the MErcury Surface, Space ENvironment, GEochemistry, and Ranging (MESSENGER) spacecraft into orbit around Mercury in March 2011, knowledge of the planet's interior was limited to its mean density and the detection of a fluid core layer via observation of the large amplitude of its forced libration in longitude [*Margot et al.*, 2007]. Earth- and spacecraft-based observations of Mercury also suggested that the surface contains relatively little iron, in contrast with the planet as a whole [e.g., *Jeanloz et al.*, 1995; *Blewett et al.*, 1997; *Robinson and Taylor*, 2001].

[3] Mercury is the only solar system body known to be in a 3:2 spin-orbit resonance. It has been known for several decades that Mercury likely occupies a Cassini state in which the axis of rotation is nearly perpendicular to the orbital plane and the spin and orbital precession rates are equal. Because of this resonant state [e.g., *Peale*, 1988; *Peale et al.*, 2002;

[1]Department of Earth, Environmental, and Planetary Sciences, Case Western Reserve University, Cleveland, Ohio, USA.
[2]Department of Physics and Astronomy, University of California, Los Angeles, Los Angeles, California, USA.
[3]Department of Earth and Space Sciences, University of California, Los Angeles, Los Angeles, California, USA.
[4]Department of Terrestrial Magnetism, Carnegie Institution of Washington, Washington, D.C., USA.
[5]Lamont-Doherty Earth Observatory, Columbia University, Palisades, New York, USA.
[6]Planetary Science Directorate, Southwest Research Institute, Boulder, Colorado, USA.
[7]Department of Earth, Ocean, and Atmospheric Sciences, University of British Columbia, Vancouver, British Columbia, Canada.
[8]Planetary Science Institute, Tucson, Arizona, USA.
[9]NASA Goddard Space Flight Center, Greenbelt, Maryland, USA.
[10]Department of Earth, Atmospheric, and Planetary Sciences, Massachusetts Institute of Technology, Cambridge, Massachusetts, USA.
[11]Department of Mineral Sciences, National Museum of Natural History, Smithsonian Institution, Washington, D.C., USA.
[12]Department of Physics, University of California, Santa Barbara, California, USA.
[13]Space Department, The Johns Hopkins Applied Physics Laboratory, Laurel, Maryland, USA.

Corresponding author: S. A. Hauck, II, Department of Earth, Environmental, and Planetary Sciences, Case Western Reserve University, Cleveland, OH, 44106 USA. (hauck@case.edu)

2169-9097/13/10.1002/jgre.20091

Margot et al., 2007], knowledge of the orientation of Mercury, the long-wavelength shape of the gravity field, and the amplitude of the forced libration together lead to estimates of the normalized polar moment of inertia, C/MR^2 (where M and R are planetary mass and radius), and the ratio of the polar moment of inertia of the solid outer shell of the planet to that of the whole planet, C_m/C. A measurement yielding a value of $C_m/C < 1$ implies that Mercury's interior hosts a liquid layer at depth that decouples the motion of the outer shell of the planet from the liquid interior on the timescale of the libration, the planet's 88-day year. The determination of the orientation of the spin axis and amplitude of the physical libration by Earth-based radar measurements [*Margot et al*., 2007] and the early estimates of the gravity field of Mercury from tracking Mariner 10 [*Anderson et al*., 1987] and later MESSENGER during its first two flybys of the planet [*Smith et al*., 2010] confirmed the existence of a molten core layer. These measurements are also important because the value of C/MR^2 is a gauge of how mass is radially distributed within the planet, whereas C_m/C is particularly sensitive to the outer radius of the liquid portion of the core.

[4] Observations of Mercury by MESSENGER's suite of sensors sensitive to the elemental and mineralogical composition of surface materials provide important additional clues to the composition of the planet's interior. Early orbital measurements by MESSENGER's X-Ray Spectrometer (XRS) [*Nittler et al*., 2011] indicated that surface material not only contains no more than ~4 wt % Fe but displays comparably low concentrations of Ti and Al as well. More recent estimates from analysis of larger sets of XRS and Gamma-Ray Spectrometer (GRS) data indicate a bulk elemental Fe content closer to ~1–2 wt % [*Evans et al*., 2012; *Weider et al*., 2013]. These observations are strongly suggestive of a relatively modest bulk density for the portions of the silicate mantle that served as source regions for magmas that supplied surface volcanic material. The XRS measurements also indicate a surface S content nearly an order of magnitude larger than for Earth or the Moon. The combination of low Fe and high S contents are consistent with Mercury having formed from highly reduced components [*Nittler et al*., 2011; *McCubbin et al*., 2012; *Zolotov et al*., 2013]. This highly reducing environment would have favored the partitioning of Si, possibly in addition to S, into the metallic materials that make up Mercury's core during global core-mantle differentiation [*McCoy et al*., 1999; *Malavergne et al*., 2010]. However, Fe–S–Si alloys display liquid immiscibility at pressures less than 15 GPa and temperatures above the liquidus temperature [e.g., *Sanloup and Fei*, 2004; *Morard and Katsura*, 2010], a situation that can lead to a buoyancy-driven segregation of the core and more S-rich material near the core-mantle boundary.

[5] Analysis of X-band Deep Space Network (DSN) tracking data of MESSENGER in orbit around Mercury resulted in the determination of a spherical harmonic model of the gravity field complete to degree and order 20. This gravity field includes the normalized low-degree harmonics pertaining to the dynamical oblateness, $C_{20} = (2.25 \pm 0.01) \times 10^{-5}$, and the dynamical equatorial ellipticity, $C_{22} = (1.253 \pm 0.01) \times 10^{-5}$, both of which depend on the internal mass distribution. The uncertainties (both of which are given by the standard deviation, σ) represent best estimates derived from an ensemble of clone models rather than formally propagated errors [*Smith et al*., 2012]. These values for the second-degree harmonics, which are derived from orbital data, supersede the values developed from two Mercury flybys by MESSENGER [*Smith et al*., 2010] and those using three Mariner 10 flybys of Mercury [*Anderson et al*., 1987]. From this estimation of Mercury's spherical harmonic gravity coefficients C_{20} and C_{22} together with prior Earth-based measurements of the planet's obliquity and libration amplitude [*Margot et al*., 2007], *Smith et al*. [2012] obtained the first joint estimates of the moment of inertia parameters $C/MR^2 = 0.353 \pm 0.017$ and $C_m/C = 0.452 \pm 0.035$. These results indicated that Mercury presently has a thin, solid outer shell 410 ± 37 km thick with an average density of 3650 ± 225 kg m^{-3}. The relatively large nominal value of this shell density, in spite of the low Fe abundance in surface materials and in concert with the strongly reducing conditions inferred for Mercury's precursory material, led *Smith et al*. [2012] to interpret the internal structure as being most consistent with models involving a core of Fe–S–Si composition. The aforementioned immiscibility and buoyancy-driven chemical segregation in Fe–S–Si alloys leads to the possibility that a layer of solid FeS may have formed at the top of the core and may now comprise a portion of Mercury's solid outer shell [*Malavergne et al*., 2010; *Smith et al*., 2012].

[6] Earth-based radar observations of Mercury through March 2012 have led to a refinement in the knowledge of the spin state of the planet, and hence its moment of inertia parameters. *Margot et al*. [2012] analyzed several additional years of observations that led to values for the obliquity of 2.04 ± 0.08 arcmin and the amplitude of the longitudinal libration of 38.5 ± 1.6 arcsec, both updates to the values given by *Margot et al*. [2007]. The new moment of inertia values are $C/MR^2 = 0.346 \pm 0.014$ and $C_m/C = 0.431 \pm 0.025$ (1σ) [*Margot et al*., 2012]. These values differ from those of *Smith et al*. [2012], though they are within one standard deviation.

[7] Here, we examine a wide range of possible internal structures for Mercury by considering a broad set of possible core compositions. We detail the modeling of the internal structure and the approach for estimating Mercury's density layering. Notably, we consider the consequences for the most recent update to knowledge of Mercury's moment of inertia parameters for the planet's internal structure [*Margot et al*., 2012]. Finally, we assess the implications of the internal structure results for Mercury's evolution.

2. Methodology

2.1. Internal Structure Modeling

[8] We model the internal density distribution of Mercury as a one-dimensional radially layered structure with two to three solid layers overlying a liquid outer core and a possible solid inner core with a methodology refined from that of *Hauck et al*. [2007]. The outermost solid layers are taken each to be of constant density. Mercury's low surface gravitational acceleration and the likely limited thickness of the planet's solid outer shell implied by the high bulk density of the planet support the assumption of constant density for

these layers. Indeed, the density within the mantle would likely increase $<100\,\mathrm{kg\,m^{-3}}$ due to the effect of pressure [*Rivoldini et al.*, 2009]. Furthermore, rather than tying the density structure to an unknown silicate composition, we investigate a wide range of possible density structures to find conservative bounds on the structure of the solid outer shell. An appropriate equation of state (EOS), dependent on composition, is implemented for the liquid outer and possible solid inner core layers. For these portions of the planet, the core is divided into 1000–2000 radial layers to capture the monotonic variation of density with depth as a result of the large variations in pressure.

[9] Successful models of Mercury's interior must first match the planet's measured bulk density and mean radius. An individual model of the internal structure is constructed by taking as fixed parameters a set of densities for the crust and (upper) mantle layers, a composition for the core, and the thicknesses of the outermost silicate layers and any inner core. By varying the radius of the boundary between the liquid outer core and the base of the solid outer shell of Mercury, we search for those radial positions that match the bulk density of the planet. In order to find the location of this boundary, it is necessary to know the density profile of the core, for which the pressure varies by a factor of approximately 5 to 10 from the top of the liquid core to the center of the planet. We implement a third-order Birch-Murnaghan EOS [e.g., *Poirier*, 2000] for the liquid outer and solid inner portions of the core that relates pressure, P, to density, ρ:

$$P = \frac{3K_0}{2}\left[\left(\frac{\rho}{\rho_0}\right)^{7/3} - \left(\frac{\rho}{\rho_0}\right)^{5/3}\right] \cdot \left[1 + \frac{3}{4}(K_0' - 4)\left\{\left(\frac{\rho}{\rho_0}\right)^{2/3} - 1\right\}\right] + \alpha_0 K_0 (T - T_0), \quad (1)$$

where T, T_0, ρ_0, K_0, K_0', and α are the local and reference temperatures, the reference density, the isothermal bulk modulus and its pressure derivative, and the reference volumetric coefficient of thermal expansion. Under hydrostatic equilibrium, the variation in pressure with radius is

$$P(r) = \int_R^r \rho(x) g(x) \mathrm{d}x, \quad (2)$$

where x is the variable of integration, R the radius of the planet, and g the acceleration of gravity as a function of radius given by

$$g(r) = \frac{4\pi G}{r^2}\int_0^r \rho(x) x^2 \mathrm{d}x \quad (3)$$

[10] We assume an adiabatic temperature profile within the liquid portion of the core and that the inner core is isothermal [*Hauck et al.*, 2007]; here we find the adiabatic profile in the liquid core by integrating

$$\frac{\mathrm{d}T}{\mathrm{d}P} = \frac{\alpha T}{\rho C_\mathrm{P}} \quad (4)$$

where C_P is the specific heat, the local density ρ is calculated from equation (1), and the local coefficient of volumetric thermal expansion α is found from the relation

$$\alpha_0 K_0 = \alpha K. \quad (5)$$

[11] The local bulk modulus is

$$K = \rho \frac{\mathrm{d}P}{\mathrm{d}\rho}. \quad (6)$$

[12] Equations (1)–(6) are solved iteratively to determine self-consistent profiles of pressure, density, and temperature.

[13] For each internal structure model that is consistent with the size and density of Mercury, we calculate the normalized moment of inertia, C/MR^2, and the fraction of the polar moment of inertia contributed by the solid outer shell of the planet, C_m/C. The mass of the planet is given by

$$M = 4\pi \int_0^R \rho(x) x^2 \mathrm{d}x. \quad (7)$$

[14] The polar moment of inertia, C, is

$$C = \frac{8\pi}{3}\int_0^R \rho(x) x^4 \mathrm{d}x, \quad (8)$$

and the portion of the polar moment of inertia due to the solid outer shell, C_m/C, is defined by

$$\frac{C_\mathrm{m}}{C} + \frac{C_\mathrm{c}}{C} = 1, \quad (9)$$

where C_c/C is the fraction of the polar moment of inertia contributed by the mass distribution below the solid outer shell. C_c is calculated from equation (8) integrated to the core-mantle boundary, and C_m/C is determined from the identity in equation (9).

2.2. Properties of Core-Forming Materials

[15] Mercury's large bulk density implies a large core, almost certainly dominated by iron. However, thermal history considerations dictate that a core composed purely of iron would be entirely solid at present [*Siegfried and Solomon*, 1974], which is inconsistent with both the detection of a core of which a portion is molten [*Margot et al.*, 2007] and a dynamo-generated magnetic field [*Anderson et al.*, 2011]. Although the precise composition of Mercury's core is unknown, iron should be alloyed with one or more light elements that act to reduce the melting temperature and density of the core, analogous to the situation in Earth's core [e.g., *Hillgren et al.*, 2000]. Sulfur has received the greatest attention in previous work on Mercury's interior due to its affinity for Fe, its cosmochemical abundance, and the large reductions in melting point and density of Fe–S alloys compared with pure Fe. MESSENGER XRS measurements of up to ~4 wt % S on the surface of Mercury are consistent with the presence of the moderately volatile sulfur in the planet's precursory materials despite Mercury's proximity to the Sun [*Nittler et al.*, 2011]. A consequence of the reducing conditions implied by the high S abundance and low Fe abundance in Mercury's silicate fraction is that elements such as silicon or carbon should alloy with iron

either in concert with or instead of sulfur [e.g., *Malavergne et al*., 2010]. Each of these elements alloys differently with Fe, and hence their material properties must be considered independently.

[16] The Fe–S system is the best characterized of the potential core-forming alloys, especially at the pressures and temperatures relevant to Mercury's core. For the pure Fe end-member, we utilize the equation of state of *Komabayashi and Fei* [2010]. Compared with previous modeling efforts [*Harder and Schubert*, 2001; *Hauck et al*., 2007; *Riner et al*., 2008; *Rivoldini et al*., 2009] that made use of earlier EOSs, particularly that of *Anderson and Ahrens* [1994] for liquid Fe, the EOS of *Komabayashi and Fei* [2010] results in relatively larger densities for Fe at the relevant pressures in Mercury's core. Following *Hauck et al*. [2007], we implement a linear parameterization of the reference parameters of the equation of state between their Fe and FeS end-members. The single exception is that the sulfur dependence of the bulk modulus is parameterized as a quadratic fit to the data of *Sanloup et al*. [2000] as a function of mass fraction of sulfur χ_S,

$$K_0 = K_{0a}\chi_S^2 + K_{0b}\chi_S + K_{0c}. \tag{10}$$

[17] In contrast with S, Si is more soluble in solid Fe and displays solid-solution behavior. Whereas on the Fe-rich side of the Fe–FeS eutectic the precipitation of solid Fe is relatively free of S, a solid precipitate from a liquid Fe–FeSi alloy will have nearly the same composition as the liquid. Indeed, experiments by *Kuwayama and Hirose* [2004] demonstrate that at 21 GPa the compositional difference between the liquid and solid is less than 2 wt %. Given that solid-liquid compositional differences are smaller than 2 wt % over most of the phase diagram, we make the simplifying assumption that solid and liquid portions of an Fe–FeSi core are the same composition. From a combination of experiments and literature data, *Dumay and Cramb* [1995] demonstrated that the molar volume of liquid Fe–Si alloys has a nonlinear dependence on the amount of Si in the alloy. Consequently, we employ a quadratic parameterization of the *Dumay and Cramb* [1995] data for the Fe–Si liquid reference density at 1723 K as a function of Si mass fraction:

$$\rho_{0,Fe\text{-}Si,1} = \rho_{0,Fe\text{-}Si,a}\chi_{Si}^2 + \rho_{0,Fe\text{-}Si,b}\chi_{Si} + \rho_{0,Fe\text{-}Si,c}. \tag{11}$$

[18] Solid Fe–Si alloys are assumed to have an EOS described by a linear dependence on the mass fraction of Si between the pure face-centered cubic (γ) phase of Fe [*Komabayashi and Fei*, 2010] and an alloy of Fe–Si with 17 wt % Si [*Lin et al*., 2003].

[19] The strong chemically reducing conditions indicated by MESSENGER XRS measurements of surface materials [*Nittler et al*., 2011] are consistent with a core containing multiple light alloying elements, likely including S and Si [*Malavergne et al*., 2010]. The Fe–S–Si ternary system is not as well characterized as the binary end-members, especially at high temperature and pressure, though experiments have demonstrated the presence of a substantial superliquidus miscibility gap that persists up to a pressure of ~15 GPa [*Sanloup and Fei*, 2004; *Morard and Katsura*, 2010]. The primary consequence of this immiscibility is that the shallow portion of Mercury's core should be dominated by buoyant, S-rich (i.e., more sulfur-rich than eutectic Fe–S) fluids. Consistent with the *Sanloup et al*. [2000] finding of a strong dependence of the Fe–S liquid alloy bulk modulus on S content, recent experiments by *Nishida et al*. [2011] indicate that liquid FeS is a soft material that is readily compressible. At the conditions of Mercury's outer core, where pressures at the top of the liquid layer are ~4–7 GPa, any solid precipitation there would likely be dominantly the high-temperature and modestly high-pressure phase of iron sulfide known as FeS V [*Fei et al*., 1995; *Urakawa et al*., 2004]. The relatively low density and heat capacity of FeS liquid lead to an adiabatic gradient greater than the melting curve gradient. Such a gradient indicates that solid FeS would likely precipitate first at the core-mantle boundary. As long as the Fe content of the S-rich liquid is a few wt % more than the FeS end-member, solid FeS should be buoyant in the residual liquid and remain at the top of the core.

2.3. Approach

[20] The estimation of the internal structure of a planet from the mass and moment of inertia relationships is an inherently non-unique process that is well suited to Monte Carlo inversion methods. In the case of Mercury, it is fortunate that the experiment to determine the state and structure of Mercury's core [*Peale et al*., 2002] yields two measures of the planet's internal structure to constrain modeling efforts. The normalized polar moment of inertia, C/MR^2, provides information on the degree to which density increases with depth. The value of C_m/C also depends upon the density distribution of the interior, though it is particularly sensitive to the location of the outermost solid-liquid boundary. Use of both C/MR^2 and C_m/C as restraints permits tighter constraints on Mercury's interior than if only C/MR^2 were known [*Hauck et al*., 2007].

[21] A particular advantage of a Monte Carlo approach is that a consistent picture emerges of the probability distribution of the recovery of parameters that describe the internal structure of Mercury. Both uncertainties in material parameters (Table 1) and in the measurements of C/MR^2, C_m/C, and the bulk density, ρ_{bulk}, of Mercury contribute to uncertainty in the internal structure. Our basic approach is to calculate large ensembles (typically of order 10^5–10^6) of internal structure models consistent with the radius and bulk density of Mercury. Each ensemble represents a particular set of assumptions regarding the composition of the core and the range of possible densities for the outermost solid layers of the planet. From an ensemble we construct a sample of the models that have a distribution relative to the central values of C/MR^2 and C_m/C consistent with their observed probability distribution, under the assumption that the uncertainties in the moment of inertia parameters are independent of each other. The estimates of C/MR^2 and C_m/C are correlated, though modestly. Regardless, the approach of assuming the parameters are independent is the more conservative approach to estimation of model parameters [*Tarantola*, 2005].

[22] Our basic approach to constructing a set of models that is reflective of the accuracy of knowledge of Mercury's moment of inertia parameters is to carefully sample a much larger set of internal structure models that are constrained only by the planet's radius and mass. By making the assumption that the uncertainties associated with C/MR^2 and C_m/C

Table 1. Parameters for Internal Structure Models[a]

Parameter	Symbol	Value	Units
Bulk density of planet	ρ_{bulk}	5430 ± 10	$\mathrm{kg\,m^{-3}}$
Radius of planet	R	2440	km
Mantle density	ρ_{m}	2800–3600	$\mathrm{kg\,m^{-3}}$
Crustal density	ρ_{crust}	2800–3600	$\mathrm{kg\,m^{-3}}$
Ratio of inner core radius to outer liquid core radius	$R_{\mathrm{ic}}/R_{\mathrm{slb}}$	0–1	–
Crustal thickness	d_{crust}	0–150	km
Thickness of solid FeS layer	d_{FeS}	0–200	km
Thickness of dense basal mantle layer	d_{basal}	0–200	km
Core-mantle boundary temperature	T_{cmb}	1700–2100	K
Density of dense basal mantle layer	ρ_{basal}	3600–5400	$\mathrm{kg\,m^{-3}}$
Solid γ Fe reference density	$\rho_{0,\mathrm{Fe,s}}$	8170 ± 82	$\mathrm{kg\,m^{-3}}$
Solid γ Fe reference temperature	$T_{0,\mathrm{Fe,s}}$	298	K
Solid γ Fe coefficient of thermal expansion	$\alpha_{0,\mathrm{Fe,s}}$	6.4×10^{-5}	$\mathrm{K^{-1}}$
Solid γ Fe bulk modulus	$K_{0,\mathrm{Fe,s}}$	165	GPa
Solid γ Fe pressure derivative of K_0	$K'_{0,\mathrm{Fe,s}}$	5.5	–
Liquid Fe reference density	$\rho_{0,\mathrm{Fe,l}}$	8069 ± 200	$\mathrm{kg\,m^{-3}}$
Liquid Fe reference temperature	$T_{0,\mathrm{Fe,l}}$	298	K
Liquid Fe coefficient of thermal expansion	$\alpha_{0,\mathrm{Fe,l}}$	9.2×10^{-5}	$\mathrm{K^{-1}}$
Liquid Fe bulk modulus	$K_{0,\mathrm{Fe,l}}$	124	GPa
Liquid Fe pressure derivative of K_0	$K'_{0,\mathrm{Fe,l}}$	5.5	–
Liquid FeS reference density	$\rho_{0,\mathrm{FeS,l}}$	3900 ± 98	$\mathrm{kg\,m^{-3}}$
Liquid FeS reference temperature	$T_{0,\mathrm{FeS,l}}$	1473	K
Liquid FeS coefficient of thermal expansion	$\alpha_{0,\mathrm{FeS,l}}$	1.1×10^{-4}	$\mathrm{K^{-1}}$
Liquid FeS pressure derivative of K_0	$K'_{0,\mathrm{FeS,l}}$	5	–
Liquid Fe–FeS bulk modulus coefficient	$K_{0\mathrm{a}}$	554	GPa
Liquid Fe–FeS bulk modulus coefficient	$K_{0\mathrm{b}}$	−391	GPa
Liquid Fe–FeS bulk modulus coefficient	$K_{0\mathrm{c}}$	81.3	GPa
Liquid Fe–Si alloy reference temperature	$T_{0,\mathrm{Fe–Si,l}}$	1723	K
Liquid Fe–Si alloy coefficient of thermal expansion	$\alpha_{0,\mathrm{Fe–Si,l}}$	9.2×10^{-5}	$\mathrm{K^{-1}}$
Liquid Fe–Si alloy reference density coefficient	$\rho_{0,\mathrm{Fe–Si,a}}$	2361	$\mathrm{kg\,m^{-3}}$
Liquid Fe–Si alloy reference density coefficient	$\rho_{0,\mathrm{Fe–Si,b}}$	−7015	$\mathrm{kg\,m^{-3}}$
Liquid Fe–Si alloy reference density coefficient	$\rho_{0,\mathrm{Fe–Si,c}}$	7079	$\mathrm{kg\,m^{-3}}$
Liquid Fe–Si alloy Si content derivative of K_0 minimum	$\mathrm{d}K_0/\mathrm{d}\chi_{\mathrm{Si}}$	−60	GPa
Liquid Fe–Si alloy Si content derivative of K_0 maximum	$\mathrm{d}K_0/\mathrm{d}\chi_{\mathrm{Si}}$	−100	GPa
Solid FeS V reference density	$\rho_{0,\mathrm{FeS,s}}$	4400 ± 110	$\mathrm{kg\,m^{-3}}$
Solid FeS V reference temperature	$T_{0,\mathrm{FeS,s}}$	1000	K
Solid FeS V coefficient of thermal expansion	$\alpha_{0,\mathrm{FeS,s}}$	10.4×10^{-5}	$\mathrm{K^{-1}}$
Solid FeS V bulk modulus	$K_{0,\mathrm{FeS,s}}$	54.3	GPa
Solid FeS V pressure derivative of K_0	$K'_{0,\mathrm{FeS,s}}$	4	–
Solid Fe—17 wt % Si reference density	$\rho_{0,\mathrm{Fe–Si17,s}}$	7147 ± 179	$\mathrm{kg\,m^{-3}}$
Solid Fe—17 wt % Si reference temperature	$T_{0,\mathrm{Fe–Si17,s}}$	300	K
Solid Fe—17 wt % Si coefficient of thermal expansion	$\alpha_{0,\mathrm{Fe–Si17,s}}$	6.4×10^{-5}	$\mathrm{K^{-1}}$
Solid Fe—17 wt % Si bulk modulus	$K_{0,\mathrm{Fe–Si17,s}}$	199	GPa
Solid Fe—17 wt % Si pressure derivative of K_0	$K'_{0,\mathrm{Fe–Si17,s}}$	5.66	–

[a]Solid and liquid Fe EOS parameters come from *Komabayashi and Fei* [2010]; liquid FeS density data are from *Kaiura and Toguri* [1979]; liquid FeS bulk moduli coefficients from *Sanloup et al*. [2002]; liquid Fe–Si EOS data are from *Dumay and Cramb* [1995], *Sanloup et al*. [2004], and *Yu and Secco* [2008]; solid FeS V data are from *Urakawa et al*. [2004]; and solid Fe–17 wt % Si data are from *Lin et al*. [2003].

are normally distributed [*Margot et al*., 2012], we can calculate p values for the hypothesis that a given individual internal structure model's moment of inertia parameters are the same as the observed values using a standard z test [*Devore*, 1995]. We use these p values to construct our sample by taking the additional step of also calculating an additional uniform random number for each internal structure model. An acceptance–rejection test is performed by keeping models when the uniform random variate is larger than the p value and rejecting the model otherwise. The result of this process is a sample, by which we mean a subset of the models that were first calculated to be constrained only by Mercury's radius and mass, for which the probability distribution of C/MR^2 and C_{m}/C values are consistent with observations. For example, Figure 1 schematically illustrates a set of sample selections from a notional set of models shown for convenience as histograms of model values of C/MR^2. Shown is the complete set of models that are consistent with the mass and radius of Mercury, along with smaller samples of that set that are consistent with C/MR^2 and C_{m}/C observations individually and, finally, simultaneously. It is this final sample that can then be used to assess the recovery of other internal structure parameters (e.g., core size) consistent with the observations as well as the uncertainty associated with the recovery.

3. Results

[23] In order to accommodate the limited constraints on Mercury's bulk composition, we investigate a broad range of possible structures. The primary controls on the internal structure in our modeling approach are the range of densities for the layers in the solid portion of the outer shell and the composition of the core, which governs its density structure. Additional parameters, such as the relative size of the inner core and the thermal structure, are not strongly correlated

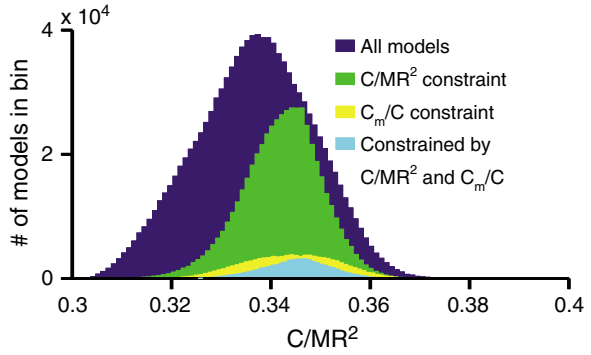

Figure 1. Schematic histograms of C/MR^2 that illustrate the construction of a sample of internal structure models consistent with the observations of C/MR^2 and C_m/C. The dark blue histogram represents all models in an ensemble, green and yellow are samples constrained by C/MR^2 and C_m/C, respectively, and light blue is a sample constrained by both moment of inertia parameters.

with the moment of inertia parameters and are simply additional sources of uncertainty in our analyses [e.g., *Hauck et al.*, 2007]. Figure 2 demonstrates the influence that core structure and composition have on the observable moment of inertia parameters by plotting samples of 200,000 individual Monte Carlo models for each of four separate ensembles. Also indicated are the nominal observed values of C/MR^2 and C_m/C (depicted as a white star) and their 1σ uncertainties. Each of these cases includes a broad range of silicate densities (2800–3600 kg m^{-3}) for both the crust and mantle layers with the constraint that the crust is less dense than the mantle. An important component of the shift in the Fe–Si models that have 0–17 wt % Si in the liquid core relative to the Fe-rich Fe–S model structures is the solid-solution behavior in Fe–Si alloys that results in nearly equal mass fractions of Si being incorporated in the solid inner core and the liquid outer core, hence limiting the density contrast across the inner core boundary (and relatively increasing C/MR^2). The right edge of each of these fields approximately corresponds to models with the highest average solid shell densities (crust plus mantle), in this case in excess of 3500 kg m^{-3}.

[24] The densities of common silicate minerals are generally proportional to their Fe content. By way of example, the orthopyroxene enstatite ($MgSiO_3$), a possible constituent of Mercury, has a density of 3200 kg m^{-3} compared with the Fe end-member ferrosilite ($FeSiO_3$) that has a density of 4000 kg m^{-3} [*Smyth and McCormick*, 1995]. Natural terrestrial peridotite samples also have a similarly large range of densities as a function of Mg number, where Mg# = Mg/(Fe + Mg) on an atomic basis [*Lee*, 2003]. Therefore, under the assumption that the relatively low Fe abundance measured in Mercury's surface materials [*Nittler et al.*, 2011] is reflective of the Fe abundance of the mantle source regions of crustal magmas [*Robinson and Taylor*, 2001], the silicate portions of the planet may be less dense than their counterparts on the other terrestrial bodies. In contrast, preliminary results based on earlier measurements of the gravity field and Earth-based observations of the spin state of Mercury plotted near, and in some cases beyond, the right edge of many of the fields in Figure 2, suggesting that the most probable density for this layer was ~3650 kg m^{-3} [*Smith et al.*, 2012]. Were terrestrial peridotites to be a reasonable analog for the source region of Mercury's crustal materials, such a density would imply an Mg# of 70 using the relationship between density and Mg# of *Lee* [2003]. Because such a large Fe content as implied by those nominal values is inconsistent with surface composition observations, *Smith et al.* [2012] considered the possibility of a deeper reservoir of dense material in the solid shell. We investigate this hypothesis further by considering a suite of cases that both do and do not lead to a deep, dense layer in the outermost solid shell. For example, as discussed previously, FeS is capable of solidifying at the top of the core for high S contents, and such a layer mechanically coupled to the mantle would increase the density of the outer solid shell of Mercury that participates in the annual libration. In the Fe–S binary system, a shallow, solid FeS layer can form from liquids more S-rich than eutectic composition, so we focus on S-rich liquid compositions of 25–36 wt % S. By constraining the density of the solid layer below the base of the silicate mantle to that described by the solid FeS V EOS at the midplane of a layer between 0 and 200 km in thickness, we can investigate the possibility of a deeper reservoir of dense material. This ensemble of models (orange dots in Figure 2) tends to larger C/MR^2 and smaller C_m/C values, and the nominal observational values of these parameters fit the observations reasonably well, at least to ~±1σ. However, although these models may be consistent with the moment of inertia parameters, such a high bulk S content would be surprising. Indeed, high core S contents are unlikely, at least in part, because the mass fraction of S relative to Fe in possible precursory analogs such as enstatite chondrites and other chondritic materials are generally insufficient to allow core sulfur contents on the FeS side of the eutectic composition.

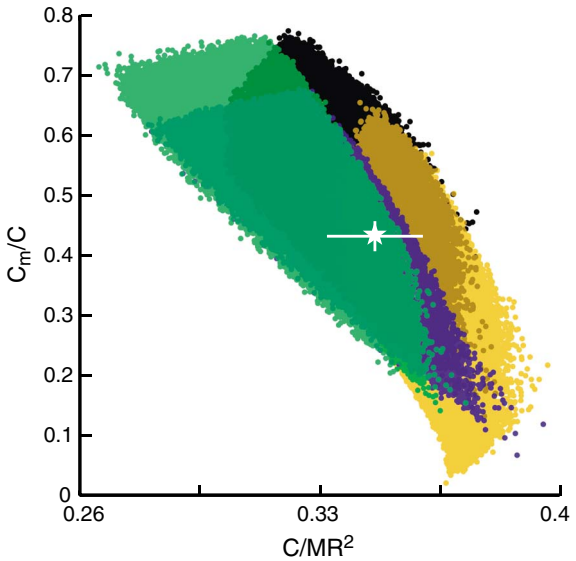

Figure 2. Comparison of ensembles of internal structure models as a function of C/MR^2 and C_m/C. Each ensemble is for a different range of core compositions. Ensembles include Fe 0–20 wt % S (green), Fe 0–17 wt % Si (blue), Fe 25–36 wt % S (orange), and Fe–S–Si (black). The white star indicates the nominal values of C/MR^2 and C_m/C, and the error bars denote 1σ uncertainties.

[25] The Fe–S–Si ternary system provides an alternative to the binary core compositional models, because under the strongly reduced conditions inferred from Mercury's surface composition [*Nittler et al.*, 2011], both S and Si can alloy with Fe, while some of the S also partitions into the silicate melt during metal-silicate differentiation [e.g., *McCoy et al.*, 1999; *Berthet et al.*, 2009; *Malavergne et al.*, 2010]. The low-pressure liquid immiscibility [e.g., *Sanloup and Fei*, 2004; *Morard and Katsura*, 2010] of the system can lead to segregation of even modest amounts of sulfur into a highly concentrated layer at the top of the core that will favor precipitation of FeS-rich solids. The efficiency of such segregation is not known, and knowledge of the details of the liquidus surface in the Fe–S–Si ternary at high pressures is limited at present. However, we can approximate the first-order consequences of segregation into, and solidification of, Si-rich and S-rich layers.

[26] We consider an Fe–Si-rich (0–17 wt% Si) region deep within the core that contains solid inner and liquid outer layer components overlain by a solid FeS layer of variable thickness between 0 and 200 km, as described previously. This approach permits consideration of a wide range of Fe–S–Si combinations, though it neglects the potential contributions of a residual Fe–S-rich liquid between the Fe–Si-rich liquid and the base of the solid FeS. However, given the limited extent of such a layer and the modest differences between the ensembles of binary Fe–S and Fe–Si liquids, the overall differences in the models are likely modest. In Figure 2, we see that the ensemble of Fe–S–Si core models matches at least as well with the observed C/MR^2 and C_m/C values as the other ensembles and may be more consistent with the reducing conditions implied by surface geochemical observations.

[27] Alternatively, we can model the deep, dense reservoir as a layer of unknown density (>3600 kg m^{-3}) and thickness. This scenario permits sequestration of higher-density and possibly more Fe-rich materials deep within the mantle that thus far do not appear to have been substantially tapped by the partial melting that yielded igneous rocks on Mercury's surface or by the formation of large basins. Such material would also likely be in chemical disequilibrium with the uppermost mantle. However, for the sake of completeness, we have calculated such an ensemble with the result that the field of possible models is widened in the plot of moment of inertia parameters, and the required average density of the silicate crust and uppermost mantle is reduced. These results are not depicted in Figure 2, as they have a very similar footprint to the field of models in black; the details of this ensemble of models are discussed further below.

[28] In order to understand the implications of the observed moment of inertia parameters for Mercury's interior, we consider each of the ensembles shown in Figure 2 as well as the ensemble that includes a dense layer at the base of mantle of unknown composition. However, we focus on the ensemble with an Fe–S–Si alloy in the core, as previously explored [*Smith et al.*, 2012], so as to obtain a sense of how the radius of the shallowest solid-liquid boundary (R_{slb}) and the bulk densities of the material above (ρ_{outer}) and below (ρ_{inner}) this boundary [*Hauck et al.*, 2007] vary with the moment of inertia parameters. These three quantities, as noted above, are the most robustly determined of the parameters that describe the internal structure of the planet. By computing large numbers of internal structure models consistent solely with Mercury's radius and bulk density, we can gain a broad perspective on

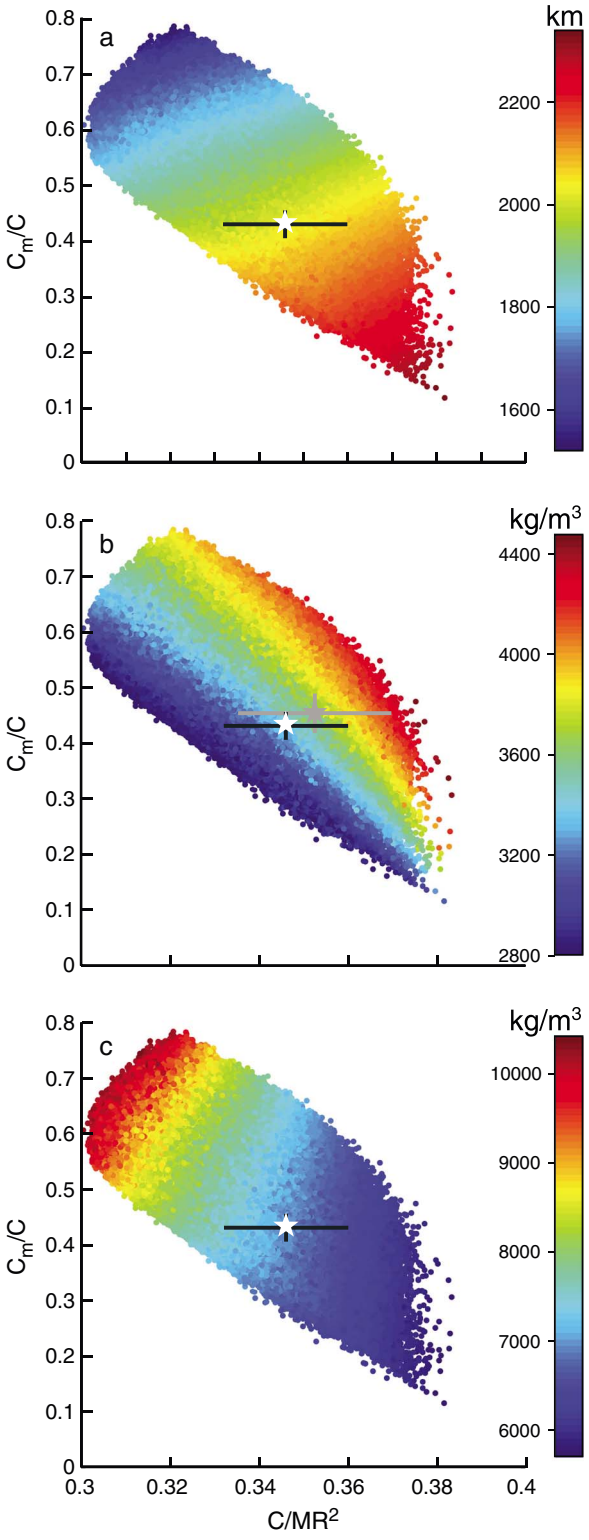

Figure 3. Plots of the Fe–S–Si ensemble for which each of the ~1 × 10^6 internal structure models consistent with the bulk density and radius of Mercury is shown as a function of C/MR^2 and C_m/C, and in color are the parameters (a) R_{slb}, (b) ρ_{outer}, and (c) ρ_{inner}. The white star indicates the nominal values of C/MR^2 and C_m/C, and the error bars are 1σ uncertainties. The gray star and error bars in Figure 3b indicate the values previously reported by *Smith et al.* [2012].

how each of these three parameters control C/MR^2 and C_m/C values and how the predictions of models compare with the observed values of the moment of inertia parameters.

[29] Indeed, C/MR^2 generally increases and C_m/C decreases with increasing R_{slb} (Figure 3a), whereas increasing the solid outer shell density ρ_{outer} (Figure 3b) leads to increases in both C/MR^2 and C_m/C. This behavior for R_{slb} is the result of increasing the proportion of the planet that is dominantly one material (i.e., the core) and reducing the overall mass gradient with depth, which acts to increase C/MR^2. Further, the proportion of the planet that is represented by the solid outer shell decreases as R_{slb} increases, thereby reducing the contribution of C_m to the planet's total polar moment of inertia, C. Similarly, the increase in C/MR^2 with increasing ρ_{outer} is the result of a decrease in the mass gradient with depth; C_m/C, however, increases with ρ_{outer} due to the increasing fraction of the mass represented by the outer shell. The effect of ρ_{inner} (Figure 3c), the density of the material deeper than R_{slb}, which comprises most of the core, is broadly similar to the effect of R_{slb} because the location of the boundary depends strongly on ρ_{inner} in order to match the bulk density of the planet. Figure 3 illustrates that, relative to the range of possible models, C_m/C is well constrained, whereas the larger fractional uncertainty on C/MR^2 and limited numerical range of possible C/MR^2 values permits a wider range of probable structural parameters. Also shown in Figure 3b is a comparison of the observed moment of inertia parameters obtained from the most recent spin-state results [*Margot et al.*, 2012] with those reported by *Smith et al.* [2012]. Clearly, the difference in C/MR^2 and C_m/C values is small, but a decrease in both parameters is most sensitive to ρ_{outer}, and hence the change in the nominal value of the shell density compared with values reported by *Smith et al.* [2012].

[30] The Monte Carlo approach to modeling the internal structure of Mercury is particularly advantageous in large part because it permits a statistical evaluation of parameter recovery. The 10^5–10^6 internal structures for any particular ensemble, i.e., each set of models with the same assumed range of core properties and silicate shell properties (each color field in Figure 2 is one ensemble) permit propagation of the uncertainty in several parameters [e.g., *Hauck et al.*, 2007]. However, it is the knowledge of Mercury's C/MR^2 and C_m/C values that most strongly limits our understanding of the planet's interior. We use samples selected from each ensemble (Figure 1) to estimate the basic parameters that describe Mercury's interior. In the figures that follow, we plot the sample consistent with the moment of inertia parameters both in terms of their fit to the nominal C/MR^2 and C_m/C values and as a histogram. Fits to these nominal parameters are shown as a function of the root mean square (RMS) of the fractional difference

$$\mathrm{RMS} = \left[\frac{1}{2}\left(\left(\frac{x_{model} - x_{obs}}{x_{obs}}\right)^2\right) + \left(\frac{y_{model} - y_{obs}}{y_{obs}}\right)^2\right]^{\frac{1}{2}} \quad (12)$$

where x and y are C/MR^2 and C_m/C, respectively. The histograms in the following figures illustrate the relevant probability distribution for each parameter, though the mean values are slightly skewed by the natural bounds on the population of possible models (i.e., the outlines of a particular ensemble

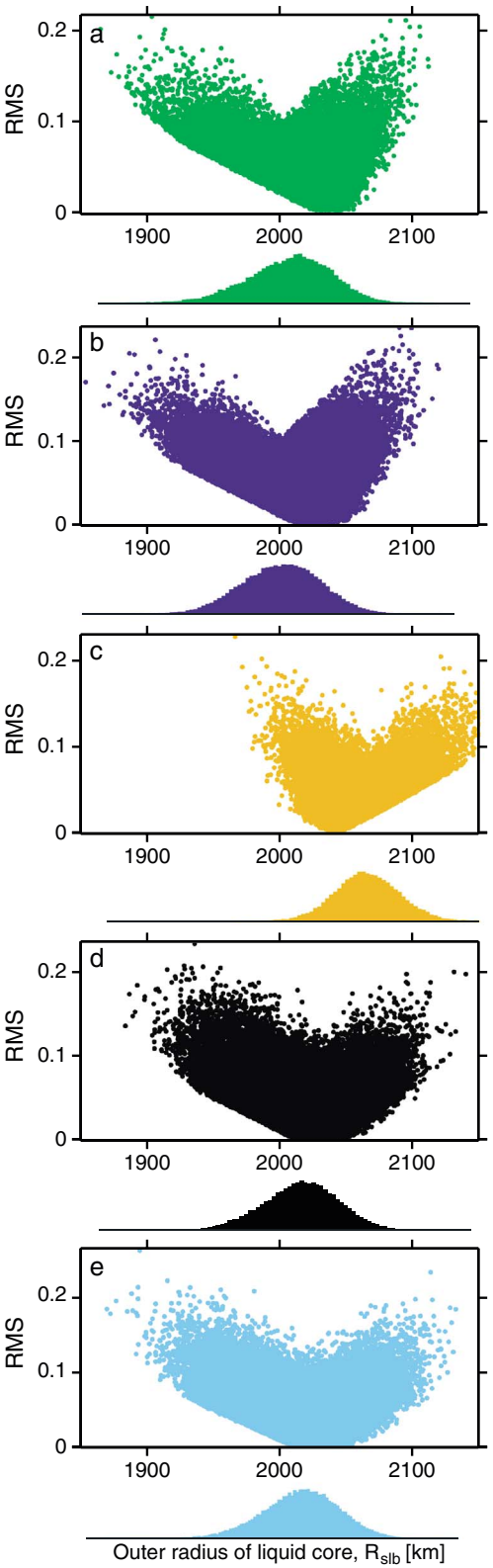

Figure 4. Outer radius of the liquid core (R_{slb}) indicated in terms of the RMS fit and as a histogram for the samples of models consistent with the measurements of C/MR^2 and C_m/C. Ensembles include (a) Fe 0–20 wt % S (green), (b) Fe 0–17 wt % Si (blue), (c) Fe 25–36 wt % S (orange), (d) Fe–S–Si (black), and (e) Fe–Si with a dense basal mantle layer (light blue).

Table 2. Summary of Internal Structure Modeling Results[a]

Model Type	Set[a]	R_{slb} (km)	ρ_{outer} (kg/m^3)	ρ_{inner} (kg/m^3)	% Planet Mass as Core Fe
Fe–S, S-poor	Full sample	2007 ± 31	3217 ± 192	7211 ± 308	63 ± 2
	RMS ≤ 0.005	2034	3437	6880	61
Fe–Si	Full sample	2001 ± 30	3210 ± 187	7250 ± 292	67 ± 3
	RMS ≤ 0.005	2022	3390	6976	65
Fe–S, S-rich	Full sample	2066 ± 25	3732 ± 183	6538 ± 185	58 ± 3
	RMS ≤ 0.005	2042	3502	6790	57
Fe–Si + FeS at CMB	Full sample	2017 ± 29	3377 ± 201	7027 ± 280	68 ± 3
	RMS ≤ 0.005	2023	3379	6982	68
Fe–Si + basal layer	Full sample	2014 ± 29	3332 ± 182	7074 ± 269	65 ± 3
	RMS ≤ 0.005	2022	3364	6997	65

[a]"Full sample" gives the mean and 1σ uncertainty of the indicated parameter for a set of models selected on the basis of the uncertainty in the moment of inertia observations (e.g., Figures 4–7). RMS ≤ 0.005 provides the mean value for a subset of the models closest to having the nominal values of C/MR^2 and C_m/C.

in Figure 2). The RMS values are insensitive to that limitation and can indicate the fit to the nominal values of C/MR^2 and C_m/C, though without much information on the uncertainties. Even among the closest-fitting models, there is a discernible spread in possible values for the internal structure parameters; we therefore define the nominal best-fitting value as the mean of models in the sample with RMS ≤ 0.005, a limit approximately equivalent to the closest-fitting 1% of models in the statistical sample.

[31] The location of the boundary between the liquid portion of the core and the overlying solid surface shell is the parameter that can be best determined from this type of analysis [*Hauck et al.*, 2007; *Riner et al.*, 2008]. Figure 4 shows the recovery of the location of this boundary, R_{slb}, for each of the five ensembles investigated. For clarity, the color scheme follows that in Figure 2, with the addition that the results shown in light blue represent the ensemble with an Fe–Si core composition and a dense layer of unspecified composition at the base of the mantle. In Figures 4a and 4b, it is apparent that the closest-fitting models in the binary, Fe-rich models have preferred core radii in the range 2020–2040 km. The sample means are approximately 2000–2010 km (Table 2), with the offset the result of the fact that the field of possible models overlaps only a portion of the range of most probable values indicated by observations (Figure 2). However, the total range of possible models out to even three standard deviations is less than 200 km, as the standard deviation is 31 and 30 km for the Fe-rich S- and Si-bearing cores, respectively. This relatively narrow range of possible core sizes is recovered regardless of the core composition and the presence or absence of a dense solid layer near the core-mantle boundary (CMB), which is the boundary between the metallic core and the silicate mantle, as seen in Figures 4c–4e and the values in Table 2. The results for S-rich Fe–S cores (Figure 4c) display a different pattern, with somewhat larger most probable values closer to 2040 km, and the sample mean is biased to larger values than for the closest-fitting models.

[32] The bulk density of the outermost solid portion of Mercury, ρ_{outer}, is also a reflection of its constituents. Figure 5 illustrates the average density of the outer solid shell of the planet for those cases modeled with a two-layer (Figures 5a and 5b) or a three-layer (Figures 5c–5e) core structure. In each ensemble, the closest-fitting models tend to have bulk densities toward the middle to upper end of the range of silicate layer densities considered. Indeed, the means of the closest-fitting models (RMS ≤ 0.005) in each ensemble are ≥ 3360 kg m^{-3}. The one standard deviation uncertainty of ρ_{outer} at $>6\%$ (1σ) is about a factor of 4 greater than that for the location of the outer radius R_{slb} of the liquid portion of the core at 1.5% (Table 2). With the exception of the S-rich Fe–S core ensemble (Figure 5c), the results for both two-layer and three-layer core cases have similar results.

[33] The recovery of the bulk density of material deeper than R_{slb}, ρ_{inner}, is indicated in Figure 6. The results pertain to any solid inner core and liquid portion of the core but exclude any metallic solid layers at the top of the metallic core. The range of possible ρ_{inner} values consistent with the measured C/MR^2 and C_m/C values across all the ensembles investigated is quite broad, from approximately 6000 kg m^{-3} to 9000 kg m^{-3}. Values for the closest-fitting models are more concentrated over 6800–7000 kg m^{-3} (Table 2). These relatively modest densities are consistent with a substantial fraction of light elements alloying with Fe in the core of Mercury. However, core compositions are less constrained than the bulk densities, with the result that with the exception of the Fe-rich Fe–S ensemble the full range of core compositions studied are consistent with the moment of inertia parameters. The exception is that S contents less than approximately 6 wt% are not observed in the Fe-rich Fe–S cases. Indeed, in all the Fe-rich core compositions, light-element concentrations deeper than R_{slb} (i.e., exclusive of any FeS layer such as in the models in Figure 6d) from the middle to the upper end of the ranges studied tend to be preferred.

[34] The origin of Mercury's large bulk density is one of the primary challenges to understanding the planet [*Solomon*, 2003], with the fundamental question focused on how the planet obtained its large ratio of metal to silicate. The observations of C/MR^2 and C_m/C refine limits on the total abundance of Fe in the planet. Results for the mass fraction of the planet contributed by Fe in the core are shown in Figure 7. For the Fe-rich compositions, the range of closest-fitting Fe fractions is approximately 60–75%, depending on the ensemble, and 1σ uncertainties are in the range 2–4% (Table 2). Though these results indicate a broad range of possible Fe abundances in the interior of Mercury, the application of the moment of inertia parameter constraints has reduced the overall uncertainty in the knowledge of Fe content, at least for a given ensemble of models. For example, Figure 8 compares histograms of the fraction of planetary mass contributed by Fe in the core for the models with an Fe–S–Si composition (i.e., Figures 4d, 5d,

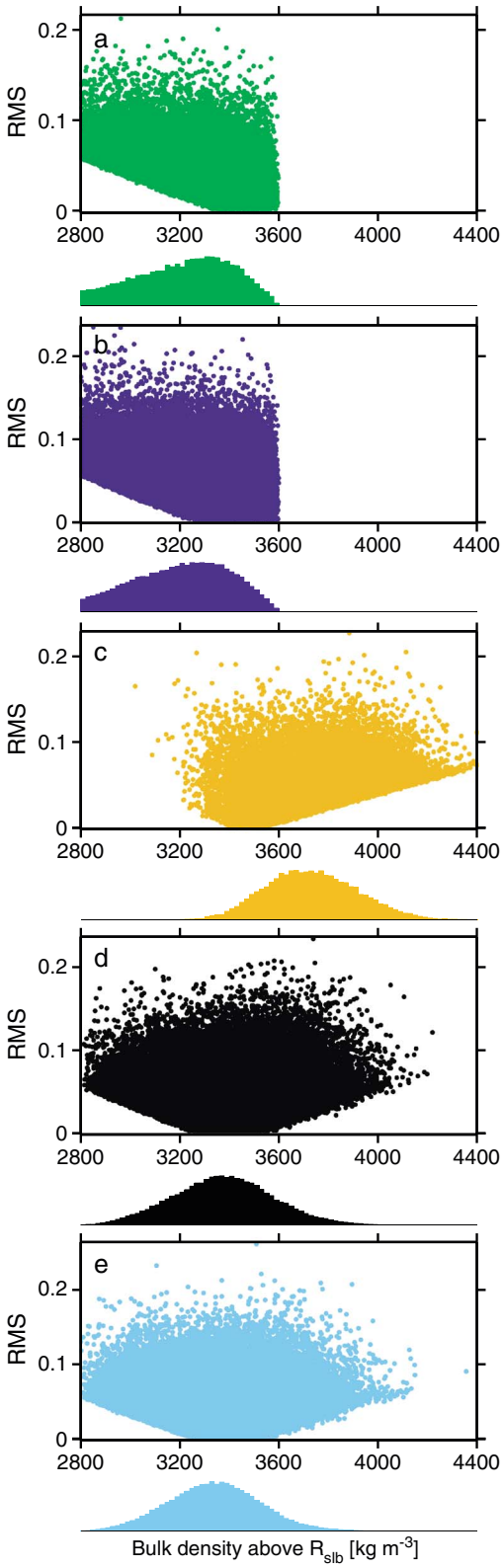

Figure 5. Bulk density of material shallower than R_{slb} (ρ_{outer}) indicated in terms of the RMS fit and as a histogram for the samples of models consistent with the measurements of C/MR^2 and C_m/C. Ensembles include (a) Fe 0–20 wt % S (green), (b) Fe 0–17 wt % Si (blue), (c) Fe 25–36 wt % S (orange), (d) Fe–S–Si (black), and (e) Fe–Si with a dense basal mantle layer (light blue).

6d, and 7d) for the entire ensemble that matches the bulk density and radius of Mercury (gray) with the sample that also matches C/MR^2 and C_m/C (black). There is a ~30% reduction in the uncertainty on the mass fraction of core Fe through the application of the moment of inertia parameters. Given the importance of constraining the amount of Fe in Mercury, this reduction is a notable improvement, and future refinements in the moment of inertia should aid in reducing further the uncertainty in the planet's bulk composition.

[35] In order to gain a fuller understanding of the limits on the internal structure of Mercury, we consider the implications of the constraints provided by the moment of inertia parameters on the properties of the core. Intertwined with the estimation of the radial density structure is the parallel estimation of pressures within the planet. Pressures within the outer solid shell of the planet are quite modest, with likely values of ~5.5 GPa at the top of the liquid core for the Fe–S–Si ensemble (Figure 9a). This figure is in contrast with nominal central pressures of ~36 GPa (Figure 9b). However, the range of possible central pressures consistent with C/MR^2 and C_m/C ranges from 30 GPa to more than 45 GPa. Mercury's variation in core pressure of a factor in the range 5–9 is the largest among the terrestrial planets. In terms of the composition and layering within the core, these parameters are less well constrained than those discussed previously, though there are interesting observations to be made. For example, in the case of a segregated Fe–S–Si core with a possible solid FeS layer at the top of the core, the observed moment of inertia parameters do not strictly constrain the thickness of the solid FeS layer d_{FeS} (Figure 10a), though it is clear that values less than ~150 km are favored both probabilistically and to a lesser extent in terms of the closest fitting models. Similar observations can be made for the Si content of the portion of the core below the solid FeS layer, in which there is a preference for the larger Si fractions modeled (Figure 10b), as well as for the size of inner core, which likely comprises less than 80% of the radius of the core below R_{slb} (Figure 10c).

4. Discussion

[36] The estimation of the two measures of Mercury's moments of inertia, C/MR^2 and C_m/C, provide crucial information on the distribution of material within the interior of the planet. Although the large bulk density of the planet by itself demands a large ratio of metal to silicate in the interior, constraints on the relative fraction have been limited. Fortunately, application of the moment of inertia parameters [*Margot et al.*, 2012] as constraints on internal structure models leads to important insights on the structure of Mercury's interior. For example, though the acknowledged uncertainty in the internal structure was quite broad, a common picture of the planet viewed the combined thickness of the silicate crust and mantle as ~600 km. The MESSENGER-derived results suggest that such a thickness is likely too high and that the more probable thickness is nearly one-third smaller. Interestingly, Fe-rich model core compositions that contain S, Si, or both lead to inferred internal structures that are broadly similar. That is, the most robust measures of the internal structure of Mercury are relatively well determined regardless of the core composition, at least for the more Fe-rich possibilities. Indeed, the mean values

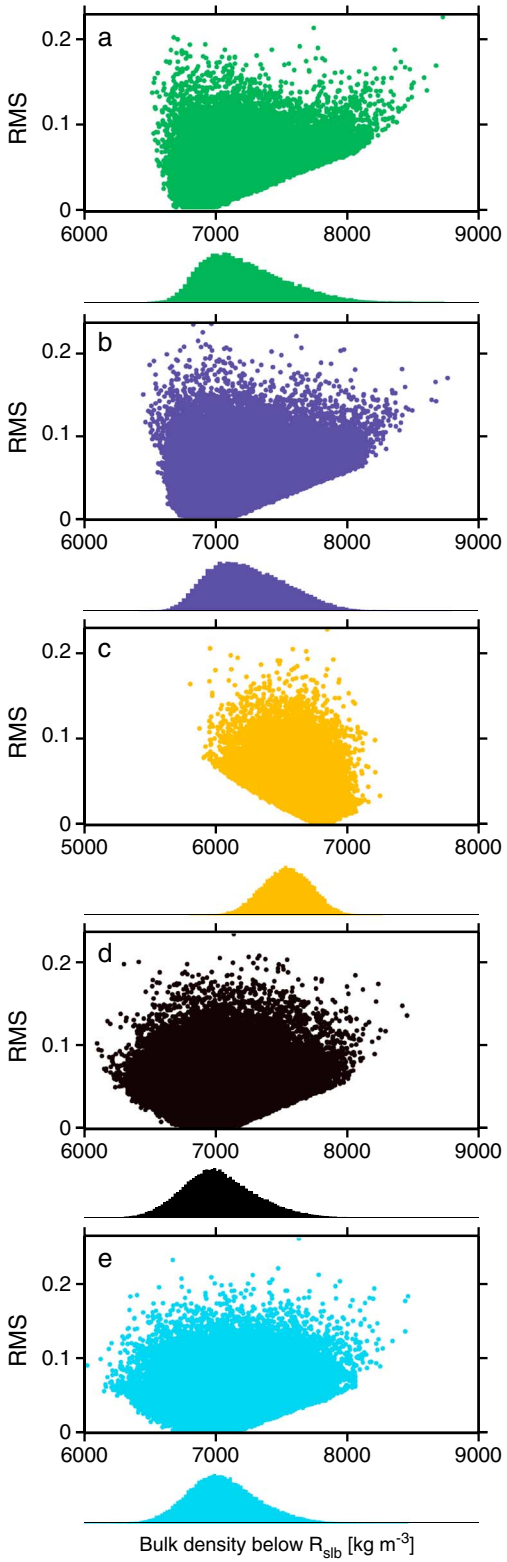

Figure 6. Bulk density of material deeper than R_{slb} (ρ_{inner}) indicated in terms of the RMS fit and as a histogram for the samples of models consistent with the measurements of C/MR^2 and C_m/C. Ensembles include (a) Fe 0–20 wt % S (green), (b) Fe 0–17 wt % Si (blue), (c) Fe 25–36 wt % S (orange), (d) Fe–S–Si (black), and (e) Fe–Si with a dense basal mantle layer (light blue). Note the shift in scale of Figure 6c relative to the other panels.

for the closest-fitting models (Table 2) of the location of the boundary between the liquid portion of the core and the overlying solid shell differ by no more than 0.6%, well within the 1σ uncertainties of ~1.5%.

[37] The Monte Carlo approach provides the opportunity to include both model parameter uncertainties (i.e., Table 1) and measurement uncertainties in the moment of inertia parameters [*Margot et al.*, 2012]. The relatively smooth variation in fundamental model parameters as compared with just the 1σ uncertainties in C/MR^2 and C_m/C underscore that it is the limits on our knowledge of the moments of inertia that continues to drive the quality of internal structure recoveries. Prior to MESSENGER's arrival in orbit around Mercury, it was the uncertainty in the gravitational field parameters C_{20} and C_{22} as determined from just three flybys each of Mercury by Mariner 10 [*Anderson et al.*, 1987] and MESSENGER [*Smith et al.*, 2010] that substantively limited our ability to estimate C/MR^2 and C_m/C accurately [*Margot et al.*, 2007; *Smith et al.*, 2010]. A series of Earth-based radar observations of Mercury over the past decade has provided an independent estimation of the rotational state of Mercury [*Margot et al.*, 2007, 2012; *Margot*, 2009] and has yielded precise values for the amplitude of the physical libration and the position of the spin pole. The latter quantity, i.e., the obliquity, remains the single largest component of uncertainty in the estimates of C/MR^2 and C_m/C at nearly 5% of the nominal value. The value of C/MR^2 is particularly sensitive to the obliquity; the leverage of C/MR^2 on the recovered density of the outer solid shell ρ_{outer} (e.g., Figure 3b) demonstrates the effect the obliquity has on the nominal outer shell density and uncertainty in internal structure. Ongoing observations by MESSENGER that combine imaging and altimetry are providing independent measurements [*Stark et al.*, 2012] of the spin state that will refine our understanding further. Indeed, a prelaunch study of the likely recovery of the gravity and spin-state parameters for a MESSENGER-like orbit suggests that just from analysis of gravity and altimeter data, knowledge of the obliquity may be capable of improvement by at least a factor of 2 [*Zuber and Smith*, 1997] over current estimates. Combination of results from multiple techniques should allow a full assessment of the obliquity and librations of Mercury and further refinement in the moment of inertia parameters.

[38] The results for Mercury's internal structure constrained by the bulk density and moment of inertia parameters for Mercury do not distinguish among possible compositions for the metallic core, particularly its complement of light alloying elements. Of course, the identity of the light element(s) even in Earth's core is debated [e.g., *Hillgren et al.*, 2000], but a common thread among efforts to deduce the internal structure of Mercury has been the assumption that the core has a composition somewhere between pure Fe and pure FeS [*Siegfried and Solomon*, 1974; *Harder and Schubert*, 2001; *Hauck et al.*, 2007; *Riner et al.*, 2008; *Rivoldini et al.*, 2009]. Sulfur is an important candidate light, alloying element in Mercury's core due to its generally siderophile nature, cosmochemical availability, and comparatively high abundance on the planet's surface [*Nittler et al.*, 2011]. However, the surface abundance combined with the low surface Fe content suggest that chemical conditions were so strongly reducing [*Nittler et al.*, 2011; *Zolotov et al.*, 2013; *McCubbin et al.*, 2012] during Mercury's formation and

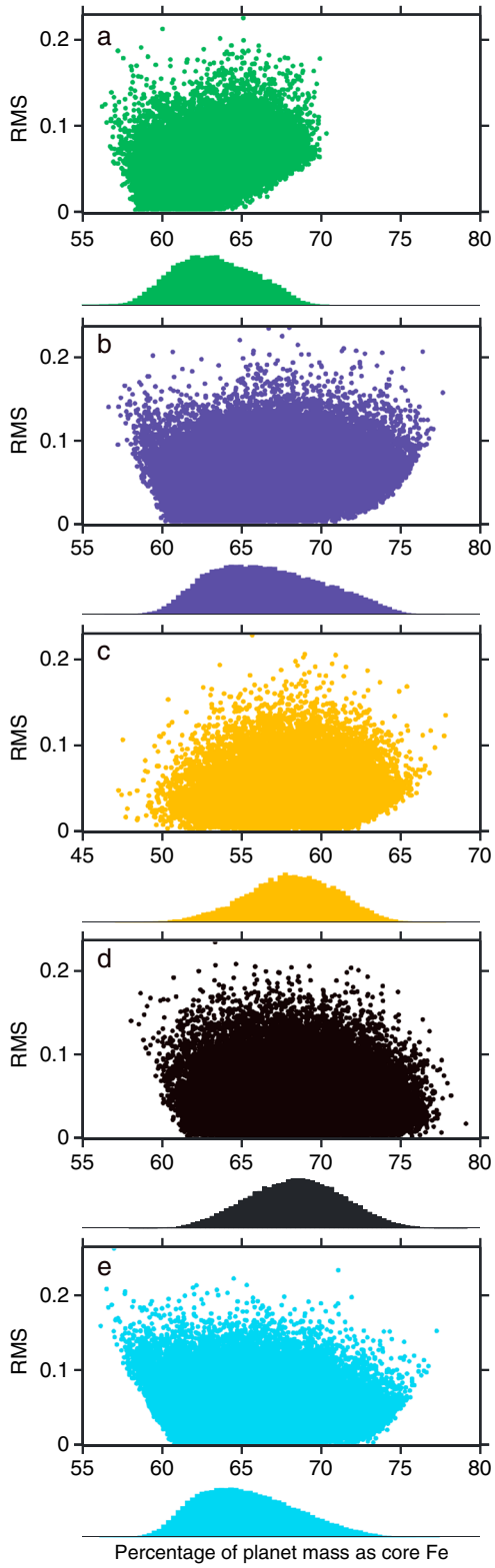

Figure 7. Percentage of the mass of Mercury contributed by Fe in the planet's core shown in terms of the RMS fit and as a histogram for the samples of models consistent with the measurements of C/MR^2 and C_m/C. Ensembles include (a) Fe 0–20 wt % S (green), (b) Fe 0–17 wt % Si (blue), (c) Fe 25–36 wt % S (orange), (d) Fe–S–Si (black), and (e) Fe–Si with a dense basal mantle layer (light blue). Note the shift in the scale of Figure 7c relative to those for the other panels.

differentiation that silicon may have also partitioned into the metallic material that formed Mercury's core. Depending on the degree of volatile loss during planet formation, carbon can also partition into metallic phases at such reducing conditions. Indeed, *McCoy et al.* [1999] observed that C-rich metallic liquids were present in 1 atm partial melting experiments on Indarch, an enstatite (EH4) chondrite and a candidate analog to precursor materials for Mercury [*Burbine et al.*, 2002; *Nittler et al.*, 2011; *Stockstill-Cahill et al.*, 2012]. More broadly, the availability of S and Si suggests that these elements may be of greater relevance to possible core compositions for Mercury.

[39] The question of the relative amounts of S and Si in Mercury's core rests with Mercury's redox state during metal-silicate separation. The solubility of Si in metallic Fe substantially increases as oxygen fugacity (fO_2) decreases and to a lesser extent as pressure increases [*Berthet et al.*, 2009]. Indeed, *Malavergne et al.* [2010] found that if Mercury's silicate FeO content were between 0.5 and 5 wt %, then the fO_2 would be between 3 and 6.5 $\log_{10}$ units below the iron-wüstite (IW) buffer or somewhat higher if ion sputtering or micrometeoroid impacts have reduced some surficial FeO to Fe. On the basis of reported MESSENGER XRS results for the elemental S and Fe contents of the surface [*Nittler et al.*, 2011], *McCubbin et al.* [2012] estimated that the redox state is between 2.6 and 6.3 $\log_{10}$ units below the IW buffer. *Zolotov et al.* [2013], who focused on understanding the origin of the large sulfur contents in surface rocks, estimate an fO_2 in the range 4.5 to 7.3 $\log_{10}$ units below the IW buffer and FeO contents <0.8 wt %. From recent partitioning experiments [*Berthet et al.*, 2009], these results imply that, depending on the average pressure of metal-silicate equilibration during separation, from 0.1 to more than 10–20 wt %, Si may alloy with Fe in Mercury's core. Furthermore, as fO_2 decreases, the S content of the silicate melts increases (i.e., S becomes more lithophile), leaving less S available to partition into the core. At least among the systems studied, there exists an approximate continuum of reducing conditions, with the Fe–S binary ensembles the least reduced, Fe–Si binary ensembles the most reduced, and the Fe–S–Si-bearing systems between the two. Within these bounds on the oxygen fugacity, it is likely that both S and Si will alloy with Fe and separate from silicates during Mercury's core-mantle differentiation [e.g., *Malavergne et al.*, 2010].

[40] Partitioning of Si into the core, with or without S, has important implications for the structure and evolution of the planet. Indeed, the immiscibility of S- and Si-rich liquids [*Sanloup et al.*, 2000; *Morard and Katsura*, 2010] at modest pressures would lead to a segregation of S-rich liquids near the top of the core with more Si-rich materials deeper, and depending on the temperatures near the CMB, crystallization of FeS-rich solids at the top of the core may have been possible. The existence of a compositionally segregated core would also place limits on the minimum mass fraction of ~6 wt % of both S and Si in order for liquid immiscibility to participate in the evolution of the core, a result generally consistent with the preference for large core Si contents (e.g., Figure 10b). Relatively reduced potential precursory materials such as EH chondrites tend to have up to 3.5 wt % Si in metal [e.g., *Keil*, 1968], implying substantial reduction of Si from the silicate precursors to Mercury's crust and mantle.

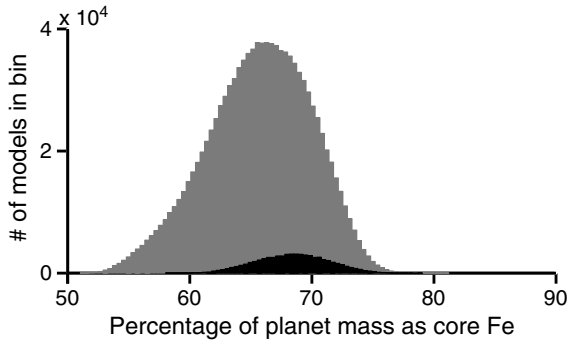

Figure 8. Histograms of the percentage of Mercury's mass contributed by Fe in the core for the entire Fe–S–Si ensemble of internal structure models that match the bulk density and radius of the planet (gray) and the sample of models that are consistent with C/MR^2 and C_m/C.

[41] The presence of a solid FeS layer at the CMB would have important consequences for mantle evolution due to the necessity for CMB temperatures to be below the solidus temperature of the FeS layer (which are in the range of 1600–1700 K depending on pressure [*Boehler*, 1992]) at present. Additionally, it is traditional for mantle convection calculations to assume a free-slip velocity boundary condition at the CMB, as the outer core is typically treated as a liquid. However, in the presence of a solid layer beneath the CMB, the more restrictive no-slip boundary condition may, depending on the layer's viscosity, be more appropriate. *Michel et al*. [2013] found that the no-slip condition affects mantle evolution modestly, but the requirement for relatively cool CMB temperatures at present is more consequential and leads in many cases to a mantle that is no longer convecting.

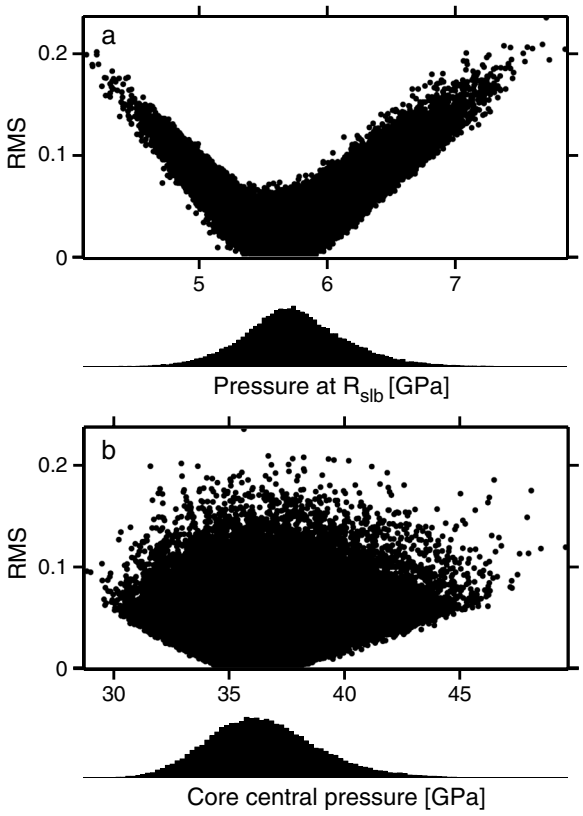

Figure 9. (a) Core-mantle boundary pressure and (b) core central pressure indicated in terms of the RMS fit and as a histogram for the samples of models consistent with the measurements of C/MR^2 and C_m/C from the Fe–S–Si ensemble of models.

[42] The compositional stratification that occurs in an Fe–S–Si core because of the immiscibility and relative density differences would also affect magnetic field generation on Mercury. A stable, electrically conductive layer beneath the CMB, either solid or liquid, would lead to attenuation of the more time-variable, short-wavelength components of any deeper dynamo-generated field via the skin-depth effect [*Christensen*, 2006]. The degree of attenuation depends on both the thickness of the layer and its electrical conductivity. Because MESSENGER observations of the long-wavelength structure of Mercury's internal magnetic field appear to be consistent with attenuation of harmonic terms of higher order than quadrupole [*Anderson et al*., 2012], such observations may provide an independent constraint on the thickness of such a layer.

[43] An important implication of a dynamo restricted to a deep region below a solid or stably stratified layer is that the inner core must be relatively small in order that the convecting region between the inner core and the nonconvecting shallowmost portion of the core will be of sufficient thickness [*Christensen*, 2006; *Christensen and Wicht*, 2008]. However, the likely Si contents deeper in the core have consequences for both the size of the inner core and the buoyancy available to drive convection. Alloys of Fe and Si form a solid solution with maximum compositional differences of ~2 wt % Si between the liquid and solid at 21 GPa [*Kuwayama and Hirose*, 2004]. As a consequence, the residual liquids are only marginally more enriched in the lighter Si component, minimizing the compositional buoyancy available to drive convection. This situation is in contrast with that for S, which has very limited solubility in solid Fe [*Li et al*., 2001], so that residual liquids have a substantial buoyancy contrast that can drive convective motions. It is worth noting that, due to the miscible nature of Fe–S–Si liquids at pressures greater than ~15 GPa (at depths ~500 km or more below R_{slb}), it is possible for any S that is not segregated to shallow levels to be preferentially expelled during inner core solidification. Regardless, the combination of the large solubility of Si in Fe metals and the smaller melting point depression of Fe–Si alloys [e.g., *Kuwayama and Hirose*, 2004] compared with Fe–S alloys [e.g., *Brett and Bell*, 1969; *Usselman*, 1975; *Fei et al*., 1997; *Li et al*., 2001; *Campbell et al*., 2007; *Stewart et al*., 2007; *Chen et al*., 2008; *Morard et al*., 2008] indicates that, relative to the commonly assumed S-bearing composition of Mercury's core [*Schubert et al*., 1988; *Harder and Schubert*, 2001; *Hauck et al*., 2004; *Hauck et al*., 2007; *Williams et al*., 2007; *Riner et al*., 2008; *Rivoldini et al*., 2009; *Grott et al*., 2011], the inner core could be larger than previously suggested. The precise difference depends on the relative amounts of both S and Si and the as yet underconstrained behavior of the liquidus in the ternary Fe–S–Si system at high pressure.

[44] The strongly reducing conditions that may partition Si into the core also have consequences for trace elements that

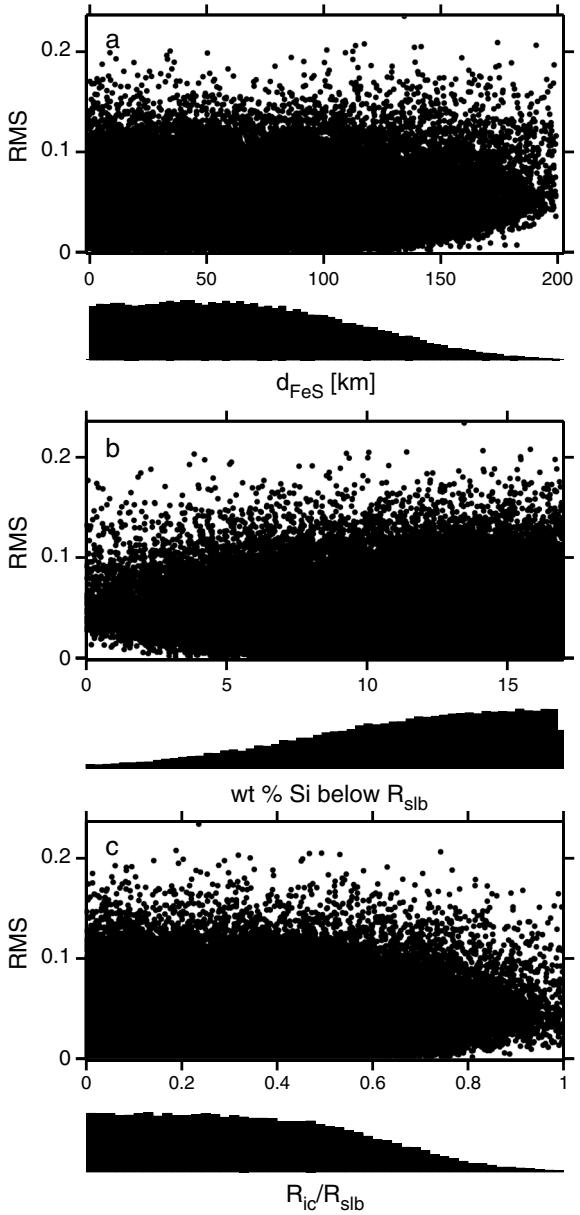

Figure 10. (a) Thickness of the solid FeS layer d_{FeS}, (b) Si content of the core deeper than the FeS layer, and (c) the radius of the inner core relative to the outer radius of the liquid core shown in terms of the RMS fit and as a histogram for the samples of models consistent with the measurements of C/MR^2 and C_m/C from the Fe–S–Si ensemble of models.

may populate the core. In particular, it appears that as fO_2 decreases the solubility of U in metal relative to silicate material tends to increase [*Malavergne et al*., 2007, 2010]. Its metal-to-silicate partition coefficient increases substantially over the range of possible fO_2 values, leading to the possibility that the outer portion of Mercury's core may host heat-producing uranium [*Malavergne et al*., 2010; *McCubbin et al*., 2012]. Data for Th are less clear, with experiments similar to those that demonstrated the fO_2 effect on U partitioning yielding no Th in the metal [*Malavergne et al*., 2010], though natural samples suggest that Th may be more chalcophilic under reducing conditions [*Malavergne et al*., 2010; *McCubbin et al*., 2012]. At the very least, MESSENGER Gamma-Ray Spectrometer measurements of surficial U and Th are inconsistent with strong partitioning of U relative to Th into Mercury's core [*Peplowski et al*., 2011]. Interestingly, K is more often invoked as a potential heat-producing element in planetary cores [*Murthy et al*., 2003; *Williams et al*., 2007]. Experiments indicate that increasing S content in the metal tends to favor an increase in K solubility as well [e.g., *Murthy et al*., 2003; *Bouhifd et al*., 2007], but decreasing fO_2 values favor decreases in the core S content that in turn imply decreases in possible K contents. Whereas the metal-to-silicate partition coefficients are relatively modest, any heat-producing elements in the core would play at least a small role in the evolution of the planet and generation of the magnetic field. For example, if the heat-producing elements were concentrated in the outer, S-rich portion of an Fe–S–Si core as suggested by *Malavergne et al*. [2010], local heat production would act to suppress the overall core cooling necessary to drive convection in the core. However, it is possible that heat production could aid convection at least within the S-rich layer, though possibly in the diffusive layering regime of double-diffusive convection (in contrast with the fingering regime, e.g., *Manglik et al*. [2010]), which may further restrict the length scale of convection. Alternatively, distribution of heat-producing elements throughout the core could act to increase entropy production in the core and aid dynamo generation [*Williams et al*., 2007]. For Fe–S–Si core compositions, the sequestration of substantial amounts of heat-producing elements in the core should slow overall core and planetary cooling and could delay the onset of the growth of a solid FeS-rich layer at the top of the core. Notwithstanding the uncertainty as to which of these effects is of greatest influence, there is an important interplay between the oxidation state of the planet Mercury, the composition and structure of the core, and the generation of the magnetic field that must be considered in understanding the planet's evolution.

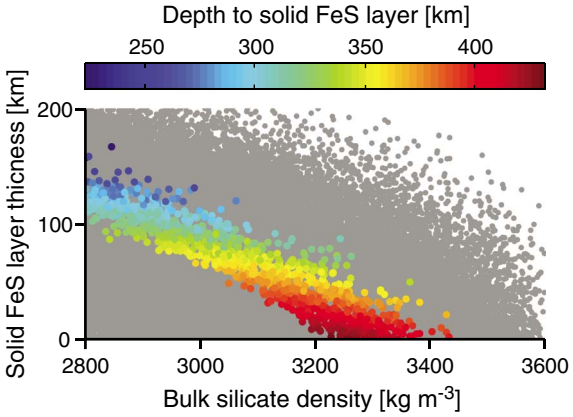

Figure 11. Tradeoffs between the thickness of the solid FeS layer and the average density of the overlying silicate material for the sample of Fe–S–Si core models consistent with C/MR^2 and C_m/C (gray) and between the thickness of the solid FeS layer and the depth to that layer for the models with RMS ≤ 0.005 (color).

[45] The possibility of an unusual structure of Mercury's core, with a liquid layer sandwiched between two solid layers due to the behavior of Fe–S–Si alloys at modest pressures, if realized, would have important implications for the nature of the planet. The thickness of any FeS layer at the top of the core and how well it might be resolved by observations are important questions. Indeed, it is R_{slb} and ρ_{outer} that are among the most robustly determined parameters, so the precise tradeoff between the thickness of the solid FeS layer, d_{FeS}, and the average density of the overlying silicates, $\rho_{silicate}$, is a crucial consideration. In Figure 11, we plot d_{FeS} against $\rho_{silicate}$ for the set of models in the Fe–S–Si ensemble that are consistent with Mercury's C/MR^2 and C_m/C. Also indicated for the set of those models with RMS ≤ 0.005 is an indication of the depth to the top of the FeS layer. Clearly, and not surprisingly given the wide set of ensembles capable of matching Mercury's moment of inertia parameters, the thickness of the FeS layer is poorly constrained (see also Figure 10a). There is, however, a clear tradeoff between the parameters for the closest-fitting models, which indicates that reduced uncertainty in the moment of inertia parameters or additional independent information on the density, makeup, or thickness of the silicate layers would yield important tests of the presence of any FeS layer. Among the closest-fitting models, it is apparent that there is a set of models that have both bulk silicate layer densities consistent with low Fe contents and have modest to negligible solid FeS layer thicknesses. Ultimately, improved constraints on the chemical character of surface materials and reduced uncertainty in rotational parameters, particularly obliquity, will narrow these possibilities further. Notably, there is a similar, though more weakly constrained tradeoff with the layer thickness for the ensemble of cases with a basal mantle layer of unspecified composition. Such a layer would likely still require a substantial Fe fraction to account for its large density, though again a set of models with a relatively small layer thickness is also consistent with the data. Here, detection of heterogeneities in Fe content across the planet's surface might be a useful test, though the accurate measurement of Fe is challenging and even more so at small spatial scales because such measurements are limited to times of strong solar flares [*Nittler et al*., 2011].

5. Summary and Conclusions

[46] The first determination of the gravity field of Mercury by a spacecraft in orbit about the planet [*Smith et al*., 2012] and new Earth-based radar observations of the planet's spin state and refinements in the planetary moment of inertia parameters [*Margot et al*., 2012] afford the opportunity to investigate anew the structure of the interior of Mercury. Through the use of Monte Carlo internal structure modeling techniques and a broad range of assumptions regarding interior composition, we have derived several constraints on the planet's internal layering. The interior is characterized by a solid outer shell overlying a metallic liquid core, and possibly a solid metallic inner core. Geochemical observations of the surface by MESSENGER are consistent with strongly chemically reducing conditions at the time of metal-silicate separation [*Nittler et al*., 2011], indicating that the metallic core may contain Si as well as possibly S as light alloying elements. Among the ensembles with Si-bearing cores (Table 2), we find that the solid outer shell of the planet is 420 ± 30 km thick and contains the silicate crust and mantle as well as a possible outer, solid portion of the core. The latter is particularly favored if the core is dominated by an Fe–S–Si alloy. In addition, the average density of the outer solid shell in these ensembles, with a nominal value of ~3380 ± 200 kg m^{-3}, is consistent with the idea that there may be a deep reservoir of dense material within the shell. With typical average core densities of 6980 ± 280 kg m^{-3}, Mercury's core likely contains a substantial quantity of light elements. The presence of an S-rich liquid at the top of Mercury's core due to immiscibility and buoyancy-driven phase separation could have important consequences for the generation of the magnetic field of the planet. Indeed, solid and potentially stably stratified portions of the liquid layer will likely limit the depth interval over which the dynamo is generated as well as preferentially attenuate the shorter-wavelength components of the field observable from orbit [e.g., *Christensen and Wicht*, 2008]. Recently obtained bounds on the contributions to Mercury's magnetic field by harmonic degrees higher than quadrupole have been interpreted as supportive of a static, electrically conducting layer overlying the dynamo-generating region of the core [*Anderson et al*., 2012]. Refinements and tests of Mercury's internal structure will come from a combination of improvements in the knowledge of the spin state and advances in understanding the generation of the planet's magnetic field, the oxidation state of its interior, and the thermodynamics of multiphase metallic systems at high pressures.

[47] **Acknowledgments.** We thank the entire MESSENGER team for the development and operation of the mission and the acquisition of the data from the first spacecraft to orbit Mercury. Discussions with Larry Nittler and Nathalie Michel on an early draft are greatly appreciated. Comments by Frank Sohl and an anonymous reviewer helped sharpen the manuscript. This work is supported by NASA MESSENGER Participating Scientist grant NNX07AR77G to S.A.H. The MESSENGER project is supported by the NASA Discovery Program under contracts NASW-00002 to the Carnegie Institution of Washington and NAS5-97271 to The Johns Hopkins University Applied Physics Laboratory. This work made use of the High Performance Computing Resource in the Core Facility for Advanced Research Computing at Case Western Reserve University.

References

Anderson, J. D., G. Colombo, P. B. Esposito, E. L. Lau, and G. B. Trager (1987), The mass, gravity field, and ephemeris of Mercury, *Icarus*, *71*, 337–349.

Anderson, B. J., C. L. Johnson, H. Korth, M. E. Purucker, R. M. Winslow, J. A. Slavin, S. C. Solomon, R. L. McNutt Jr., J. M. Raines, and T. H. Zurbuchen (2011), The global magnetic field of Mercury from MESSENGER orbital observations, *Science*, *333*, 1859–1862, doi:10.1126/science.1211001.

Anderson, B. J., C. L. Johnson, H. Korth, R. M. Winslow, J. E. Borovsky, M. E. Purucker, J. A. Slavin, S. C. Solomon, M. T. Zuber, and R. L. McNutt, Jr. (2012), Critical examination of the low-degree structure in Mercury's planetary magnetic field, *J. Geophys. Res.*, *117*, E00L12, doi:10.1029/2012JE04159.

Anderson, W. W., and T. J. Ahrens (1994), An equation of state for liquid iron and implications for the Earth's core, *J. Geophys. Res.*, *99*, 4273–4284.

Berthet, S., V. Malavergne, and K. Righter (2009), Melting of the Indarch meteorite (EH4 chondrite) at 1 GPa and variable oxygen fugacity: Implications for early planetary differentiation processes, *Geochim. Cosmochim. Acta*, *73*, 6402–6420, doi:10.1016/j.gca.2009.07.030.

Blewett, D. T., P. G. Lucey, B. R. Hawke, G. G. Ling, and M. S. Robinson (1997), A comparison of Mercurian reflectance and spectral quantities with those of the Moon, *Icarus*, *129*, 217–231, doi:10.1006/icar.1997.5785.

Boehler, R. (1992), Melting of the Fe–FeO and the Fe–FeS systems at high pressure: Constraints on core temperatures, *Earth Planet. Sci. Lett.*, *111*, 217–227.

Bouhifd, M. A., L. Gautron, N. Bolfan-Casanova, V. Malavergne, T. Hammouda, D. Andrault, and A. P. Jephcoat (2007), Potassium partitioning into molten iron alloys at high-pressure: Implications for Earth's core, *Phys. Earth Planet. Inter.*, *160*, 22–33, doi:10.1016/j.pepi.2006.08.005.

Brett, R., and P. M. Bell (1969), Melting relations in the Fe-rich portion of the system Fe–FeS at 30 kb pressure, *Earth Planet. Sci. Lett.*, *6*, 479–482, doi:10.1016/0012-821X(69)90119-8.

Burbine, T. H., T. J. McCoy, L. R. Nittler, G. K. Benedix, E. A. Cloutis, and T. L. Dickinson (2002), Spectra of extremely reduced assemblages: Implications for Mercury, *Meteorit. Planet. Sci.*, *37*, 1233–1244.

Campbell, A. J., C. T. Seagle, D. L. Heinz, G. Shen, and V. B. Prakapenka (2007), Partial melting in the iron–sulfur system at high pressure: A synchrotron X-ray diffraction study, *Phys. Earth Planet. Inter.*, *162*, 119–128, doi:10.1016/j.pepi.2007.04.001.

Chen, B., J. Li, and S. A. Hauck, II (2008), Non-ideal liquidus curve in the Fe–S system and Mercury's snowing core, *Geophys. Res. Lett.*, *35*, L07201, doi:10.1029/2008gl033311.

Christensen, U. R. (2006), A deep dynamo generating Mercury's magnetic field, *Nature*, *444*, 1056–1058, doi:10.1038/nature05342.

Christensen, U., and J. Wicht (2008), Models of magnetic field generation in partly stable planetary cores: Applications to Mercury and Saturn, *Icarus*, *196*, 16–34.

Devore, J. L. (1995), *Probability and Statistics for Engineering and the Sciences*, 4th ed., 743 pp., Duxbury Press, Belmont.

Dumay, C., and A. W. Cramb (1995), Density and interfacial tension of liquid Fe-Si alloys, *Metall. Mater. Trans. B*, *26*, 173–176.

Evans, L. G., et al. (2012), Major-element abundances on the surface of Mercury: Results from the MESSENGER Gamma-Ray Spectrometer, *J. Geophys. Res.*, *117*, E00L07, doi:10.1029/2012JE004178.

Fei, Y., C. T. Prewitt, H. K. Mao, and C. M. Bertka (1995), Structure and density of FeS at high pressure and high temperature and the internal structure of Mars, *Science*, *268*, 1892–1894.

Fei, Y., C. M. Bertka, and L. W. Finger (1997), High-pressure iron sulfur compound, Fe_3S_2, and melting relations in the Fe–FeS system, *Science*, *275*, 1621–1623.

Grott, M., D. Breuer, and M. Laneuville (2011), Thermo-chemical evolution and global contraction of Mercury, *Earth Planet. Sci. Lett.*, *307*, 135–146.

Harder, H., and G. Schubert (2001), Sulfur in Mercury's core?, *Icarus*, *151*, 118–122, doi:10.1006/icar.2001.6586.

Hauck, S. A., II, A. J. Dombard, R. J. Phillips, and S. C. Solomon (2004), Internal and tectonic evolution of Mercury, *Earth Planet. Sci. Lett.*, *222*, 713–728.

Hauck, S. A., II, S. C. Solomon, and D. A. Smith (2007), Predicted recovery of Mercury's internal structure by MESSENGER, *Geophys. Res. Lett.*, *34*, L18201, doi:10.1029/2007gl030793.

Hillgren, V. J., C. K. Gessmann, and J. Li (2000), An experimental perspective on the light element in the Earth's core, in *Origin of the Earth and Moon*, edited by R. M. Canup, and K. Righter, pp. 245–263, University of Arizona Press, Tucson.

Jeanloz, R., D. L. Mitchell, A. L. Sprague, and I. de Pater (1995), Evidence for a basalt-free surface on Mercury and implications for internal heat, *Science*, *268*, 1455–1457.

Kaiura, G. H., and J. M. Toguri (1979), Densities of the molten FeS, FeS–Cu_2S and Fe–S–O systems—Utilizing a bottom balance archimedean technique, *Can. Metall. Quart.*, *18*, 155–164.

Keil, K. (1968), Mineralogical and chemical relationships among enstatite chondrites, *J. Geophys. Res.*, *73*, 6945–6976.

Komabayashi, T., and Y. Fei (2010), Internally consistent thermodynamic database for iron to the Earth's core conditions, *J. Geophys. Res.*, *115*, B03202, doi:10.1029/2009jb006442.

Kuwayama, Y., and K. Hirose (2004), Phase relations in the system Fe–FeSi at 21 GPa, *Am. Mineral.*, *89*, 273–276.

Lee, C.-T. A. (2003), Compositional variation of density and seismic velocities in natural peridotites at STP conditions: Implications for seismic imaging of compositional heterogeneities in the upper mantle, *J. Geophys. Res.*, *108*, 2441, doi:10.1029/2003JB002413.

Li, J., Y. Fei, H. K. Mao, K. Hirose, and S. R. Shieh (2001), Sulfur in the Earth's inner core, *Earth Planet. Sci. Lett.*, *193*, 509–514.

Lin, J.-F., A. J. Campbell, D. L. Heinz, and G. Shen (2003), Static compression of iron–silicon alloys: Implications for silicon in the Earth's core, *J. Geophys. Res.*, *108*, 2045, doi:10.1029/2002jb001978.

Malavergne, V., M. Tarrida, R. Combes, H. Bureau, J. Jones, and C. Schwandt (2007), New high-pressure and high-temperature metal/silicate partitioning of U and Pb: Implications for the cores of the Earth and Mars, *Geochim. Cosmochim. Acta*, *71*, 2637–2655, doi:10.1016/j.gca.2007.03.011.

Malavergne, V., M. J. Toplis, S. Berthet, and J. Jones (2010), Highly reducing conditions during core formation on Mercury: Implications for internal structure and the origin of a magnetic field, *Icarus*, *206*, 199–209.

Manglik, A., J. Wicht, and U. R. Christensen (2010), A dynamo model with double diffusive convection for Mercury's core, *Earth Planet. Sci. Lett.*, *289*, 619–628, doi:10.1016/j.epsl.2009.12.007.

Margot, J. L. (2009), A Mercury orientation model including non-zero obliquity and librations, *Celest. Mech. Dyn. Astron.*, *105*, 329–336, doi:10.1007/s10569-009-9234-1.

Margot, J. L., S. J. Peale, R. F. Jurgens, M. A. Slade, and I. V. Holin (2007), Large longitude libration of Mercury reveals a molten core, *Science*, *316*, 710–714, doi:10.1126/science.1140514.

Margot, J. L., S. J. Peale, S. C. Solomon, S. A. Hauck, II, F. D. Ghigo, R. F. Jurgens, M. Yseboodt, J. D. Giorgini, S. Padovan, and D. B. Campbell (2012), Mercury's moment of inertia from spin and gravity data, *J. Geophys. Res.*, *117*, E00L09, doi:10.1029/2012JE004161.

McCoy, T. J., T. L. Dickinson, and G. E. Lofgren (1999), Partial melting of the Indarch (EH4) meteorite: A textural, chemical, and phase relations view of melting and melt migration, *Meteorit. Planet. Sci.*, *34*, 735–746.

McCubbin, F. M., M. A. Riner, K. E. Vander Kaaden, and L. K. Burkemper (2012), Is Mercury a volatile-rich planet?, *Geophys. Res. Lett.*, *39*, L09202, doi:10.1029/2012gl051711.

Michel, N. C., S. A. Hauck, II, S. C. Solomon, R. J. Phillips, J. H. Roberts, and M. T. Zuber (2013), Thermal evolution of Mercury as constrained by MESSENGER observations, *J. Geophys. Res. Planets*, *118*, doi:10.1002/jgre.20049.

Morard, G., and T. Katsura (2010), Pressure–temperature cartography of Fe–S–Si immiscible system, *Geochim. Cosmochim. Acta*, *74*, 3659–3667.

Morard, G., D. Andrault, N. Guignot, C. Sanloup, M. Mezouar, S. Petitgirard, and G. Fiquet (2008), In situ determination of Fe–Fe_3S phase diagram and liquid structural properties up to 65 GPa, *Earth Planet. Sci. Lett.*, *272*, 620–626.

Murthy, V. R., W. van Westrenen, and Y. Fei (2003), Experimental evidence that potassium is a substantial radioactive heat source in planetary cores, *Nature*, *423*, 163–165.

Nishida, K., E. Ohtani, S. Urakawa, A. Suzuki, T. Sakamaki, H. Terasaki, and Y. Katayama (2011), Density measurement of liquid FeS at high pressures using synchrotron X-ray absorption, *Am. Mineral.*, *96*, 864–868, doi:10.2138/am.2011.3616.

Nittler, L. R., et al. (2011), The major-element composition of Mercury's surface from MESSENGER X-ray spectrometry, *Science*, *333*, 1847–1850, doi:10.1126/science.1211567.

Peale, S. J. (1988), The rotational dynamics of Mercury and the state of its core, in *Mercury*, edited by F. Vilas, C. R. Chapman and M. S. Matthews, pp. 461–493, University of Arizona Press, Tucson.

Peale, S. J., R. J. Phillips, S. C. Solomon, D. E. Smith, and M. T. Zuber (2002), A procedure for determining the nature of Mercury's core, *Meteorit. Planet. Sci.*, *37*, 1269–1283.

Peplowski, P. N., et al. (2011), Radioactive elements on Mercury's surface from MESSENGER: Implications for the planet's formation and evolution, *Science*, *333*, 1850–1852, doi:10.1126/science.1211576.

Poirier, J. P. (2000), *Introduction to the Physics of the Earth's Interior*, 2nd ed., 312 pp., Cambridge University Press, Cambridge, U.K.

Riner, M. A., C. R. Bina, M. S. Robinson, and S. J. Desch (2008), Internal structure of Mercury: Implications of a molten core, *J. Geophys. Res.*, *113*, E08013, doi:10.1029/2007je002993.

Rivoldini, A., T. Van Hoolst, and O. Verhoeven (2009), The interior structure of Mercury and its core sulfur content, *Icarus*, *201*, 12–30, doi:10.1016/j.icarus.2008.12.020.

Robinson, M. S., and G. J. Taylor (2001), Ferrous oxide in Mercury's crust and mantle, *Meteorit. Planet. Sci.*, *36*, 841–847.

Sanloup, C., and Y. Fei (2004), Closure of the Fe–S–Si liquid miscibility gap at high pressure, *Phys. Earth Planet. Inter.*, *147*, 57–65.

Sanloup, C., F. Guyot, P. Gillet, G. Fiquet, M. Mezaouar, and I. Martinez (2000), Density measurements of liquid Fe–S alloys at high-pressure, *Geophys. Res. Lett.*, *27*, 811–814.

Sanloup, C., G. Fiquet, E. Gregoryanz, G. Morard, and M. Mezouar (2004), Effect of Si on liquid Fe compressibility: Implications for sound velocity in core materials, *Geophys. Res. Lett.*, *31*, L07604, doi:10.1029/2004GL019526.

Schubert, G., M. N. Ross, D. J. Stevenson, and T. Spohn (1988), Mercury's thermal history and the generation of its magnetic field, in *Mercury*, edited by F. Vilas, C. R. Chapman and M. S. Matthews, pp. 429–460, University of Arizona Press, Tucson.

Siegfried, R. W., II, and S. C. Solomon (1974), Mercury: Internal structure and thermal evolution, *Icarus*, *23*, 192–205.

Smith, D. E., et al. (2010), The equatorial shape and gravity field of Mercury from MESSENGER flybys 1 and 2, *Icarus*, *209*, 88–100, doi:10.1016/j.icarus.2010.04.007.

Smith, D. E., et al. (2012), Gravity field and internal structure of Mercury from MESSENGER, *Science*, *336*, 214–217, doi:10.1126/science.1218809.

Smyth, J. R., and T. C. McCormick (1995), Crystallographic data for minerals, in *Mineral Physics and Crystallography: A Handbook of Physical Constants*, edited by T. J. Ahrens, pp. 1–17, American Geophysical Union, Washington, D.C.

Solomon, S. C. (2003), Mercury: The enigmatic innermost planet, *Earth Planet. Sci. Lett.*, *216*, 441–455, doi:10.1016/s0012-821x(03)00546-6.

Stark, A., J. Oberst, F. Preusker, K. Gwinner, S. J. Peale, J.-L. Margot, M. T. Zuber, and S. C. Solomon (2012), A technique for measurements of physical librations from orbiting spacecraft: Application to Mercury, *European Planetary Science Congress 2012 Abstracts*, *7*, EPSC2012-2254.

Stewart, A. J., M. W. Schmidt, W. van Westrenen, and C. Liebske (2007), Mars: A new core-crystallization regime, *Science*, *316*, 1323–1325, doi:10.1126/science.1140549.

Stockstill-Cahill, K. R., T. J. McCoy, L. R. Nittler, S. Z. Weider, and S. A. Hauck, II (2012), Magnesium-rich crustal compositions on Mercury: Implications for magmatism from petrologic modeling, *J. Geophys. Res.*, *117*, E00L15, doi:10.1029/2012JE004140.

Tarantola, A. (2005), *Inverse Problem Theory and Methods for Model Parameter Estimation*, 342 pp., Society for Industrial and Applied Mathematics, Philadelphia, Penn.

Urakawa, S., K. Someya, H. Terasaki, T. Katsura, S. Yokoshi, K.-I. Funakoshi, W. Utsumi, Y. Katayama, Y.-I. Sueda, and T. Irifune (2004), Phase relationships and equations of state for FeS at high pressures and temperatures and implications for the internal structure of Mars, *Phys. Earth Planet. Inter.*, *143–144*, 469–479.

Usselman, T. M. (1975), Experimental approach to the state of the core; Part I, The liquidus relations of the Fe-rich portion of the Fe–Ni–S system from 30 to 100 kb, *Am. J. Sci.*, *275*, 278–290.

Weider, S. Z., L. R. Nittler, R. D. Starr, and S. C. Solomon (2013), The distribution of iron on the surface of Mercury from MESSENGER X-Ray Spectrometer measurements, *Lunar Planet. Sci., 44*, abstract 2189.

Williams, J. P., O. Aharonson, and F. Nimmo (2007), Powering Mercury's dynamo, *Geophys. Res. Lett.*, *34*, L21201, doi:10.1029/2007GL031164.

Yu, X., and R. A. Secco (2008), Equation of state of liquid Fe–17 wt % Si to 12 GPa, *High Pressure Res.*, *28*, 19–28.

Zolotov, M. Y., A. L. Sprague, S. A. Hauck, II, L. R. Nittler, S. C. Solomon, and S. Z. Weider (2013), The redox state, FeO content, and origin of sulfur-rich magmas on Mercury, *J. Geophys. Res.*, *118*, 138–146, doi:10.1029/2012JE4274.

Zuber, M. T., and D. E. Smith (1997), Remote sensing of planetary librations from gravity and topography data: Mercury simulation, *Lunar Planet Sci., 28*, abstract 1542.